Article

Fetal hepatocytes protect the HSPC genome via fetuin-A

https://doi.org/10.1038/s41586-024-08307-x

Received: 4 January 2023

Accepted: 30 October 2024

Published online: 4 December 2024

Open access

Check for updates

Xiao-Lin Guo[1,13], Yi-Ding Wang[1,13], Yan-Jun Liu[1,13], Lei Chu[2], Hua Zhu[3], Ye Hu[1], Ren-Yan Wu[1], Hong-Yu Xie[1], Juan Yu[4], Shui-Ping Li[1], Zhao-Yang Xiong[4], Ruo-Yan Li[5], Fang Ke[1], Lei Chen[6], Guo-Qiang Chen[1,7,8], Liang Chen[9], Fan Bai[5], Tariq Enver[10], Guo-Hong Li[4], Huai-Fang Li[2] & Deng-Li Hong[1,7,11,12] ✉

The maintenance of genomic integrity in rapidly proliferating cells is a substantial challenge during embryonic development[1–3]. Although numerous cell-intrinsic mechanisms have been revealed[4–7], little is known about genome-protective effects and influences of developmental tissue microenvironments on tissue-forming cells. Here we show that fetal liver hepatocytes provide protection to haematopoietic stem and progenitor cell (HSPC) genomes. Lineage tracing and depletion in mice demonstrated that delayed hepatocyte development in early fetal livers increased the chromosomal instability of newly colonizing HSPCs. In addition, HSPCs developed tolerance to genotoxins in hepatocyte-conditioned medium, suggesting that hepatocytes protect the HSPC genome in a paracrine manner. Proteomic analyses demonstrated the enrichment of fetuin-A in hepatocyte-conditioned medium but not in early fetal livers. Fetuin-A activates a Toll-like receptor pathway to prevent pathogenic R-loop accumulation in HSPCs undergoing DNA replication and gene transcription in the fetal liver. Numerous haematopoietic regulatory genes frequently involved in leukaemogenic mutations are associated with R-loop-enriched regions. In *Fetua*-knockout mice, HSPCs showed increased genome instability and susceptibility to malignancy induction. Moreover, low concentrations of fetuin-A correlated with the oncogenesis of childhood leukaemia. Therefore, we uncover a mechanism operating in developmental tissues that offers tissue-forming cell genome protection and is implicated in developmental-related diseases.

Embryonic development requires the extensive proliferation of three germinal layers that generate various functional cell types. A crucial element of developmental homeostasis is the preservation of genomic integrity during DNA replication and cellular activity through gene transcription[1–3]. Although a multitude of intrinsic cellular mechanisms for maintaining genome integrity have been extensively examined[4–7], little is known about how the tissue microenvironment safeguards tissue-forming cells from DNA damage and genome instability caused by endogenous (for example, metabolic) or exogenous genotoxic agents during development. In this study, we have demonstrated that hepatocytes have a paracrine role in providing genome protection to HSPCs in the fetal liver, the primary site of hepatogenesis and haematopoiesis[8–10].

Hepatogenesis in mice begins during embryonic days 9.0–9.5 (E9.0–9.5), as a liver bud composed of proliferating endodermal cells derived from the ventral wall of the foregut within the septum transversum[11]. Initially, the liver bud forms a solid sheet of epithelial cells, which then proliferate and branch out to form hepatic cords by E10.0–10.5. Endothelial cells originating from vitelline veins, the first vascular connection to the fetal liver, generate capillary-like sinusoids that separate the hepatic cords. By E11.5, the liver primarily consists of hepatic cords and sinusoids. HSPCs from the aorta–gonad–mesonephros region and placenta travel through umbilical vessels when the umbilical veins connect to the liver vascular system and enter the liver at E12.5. From this point forwards, the fetal liver becomes the main organ involved in fetal haematopoiesis[12]. At E13.5, approximately 75% of the liver is occupied by haematopoietic cells, a plateau that continues until E15.5, when HSPCs start migrating to the bone marrow and haematopoiesis begins to decline. During the plateau stage of haematopoiesis in the liver, hepatoblasts are separated by a high density of haematopoietic

[1]Key Laboratory of Cell Differentiation and Apoptosis of Ministry of Education, Department of Pathophysiology, Shanghai Institute of Haematology, Ruijin Hospital, Shanghai Jiao Tong University School of Medicine, Shanghai, China. [2]Department of Obstetrics and Gynecology, Shanghai Tongji Hospital, Tongji University School of Medicine, Shanghai, China. [3]Shanghai Children's Medical Center, Shanghai Jiao Tong University School of Medicine, Shanghai, China. [4]National laboratory of Biomacromolecules, Institute of Biophysics, Chinese Academy of Sciences, Beijing, China. [5]Biomedical Pioneering Innovation Centre (BIOPIC) and Translational Cancer Research Centre, School of Life Sciences, First Hospital, Peking University, Beijing, China. [6]Shanghai Institute of Immunology, Shanghai Jiao Tong University School of Medicine, Shanghai, China. [7]Research Units of Stress and Tumor, Chinese Academy of Medical Sciences, Shanghai Jiao Tong University School of Medicine, Shanghai, China. [8]Hainan Academy of Medical Sciences, School of Basic Medicine and Life Science, Hainan Medical University, Haikou, China. [9]RNA Institute, Hubei Key Laboratory of Cell Homeostasis, College of Life Sciences, Wuhan University, Wuhan, China. [10]Department of Cancer Biology, UCL Cancer Institute, University College London, London, UK. [11]Innovative Research Team of High-level Local Universities in Shanghai, Shanghai, China. [12]Shanghai Key Laboratory of Reproductive Medicine, Shanghai Jiao Tong University School of Medicine, Shanghai, China. [13]These authors contributed equally: Xiao-Lin Guo, Yi-Ding Wang, Yan-Jun Liu. ✉e-mail: dlhong@sjtu.edu.cn

cells, but at E15.5–16.5, they return to close contact with each other. As haematopoiesis decreases, hepatogenesis intensifies. By E18.5, the principal sites for haematopoiesis shift from the liver to the bone marrow[12]. Among the various developmental organs and tissues, the fetal liver is selected as the primary site for haematopoiesis, probably due to its unique microenvironment that supports both haematopoiesis and hepatogenesis. Hepatocytes and HSPCs are mutually dependent on growth and functional maintenance, as supported by our own observations and other studies[13,14]. Fetal hepatocytes are presumed to have a key role in maintaining the genome integrity of HSPCs. Our current research has revealed that fetal hepatocytes secrete fetuin-A (FetuA; also known as the α2-Heremans–Schmid glycoprotein in humans)[15,16], to protect the genome of HSPCs by preventing the accumulation of pathogenic R-loops (three-stranded structures that have an RNA–DNA hybrid). However, this protection is lacking during the early developmental stage of the fetal liver.

HSPC genomes are unstable in the early fetal liver

To assess the sensitivity of fetal HSPCs to genotoxic agents such as etoposide (Eto) and ultraviolet light (UV), we harvested HSPCs with negative lineage phenotypes and positive Sca-1 and Kit phenotypes (Lin^-, $Sca\text{-}1^+$ and Kit^+ (LSK)) from E12.5 placentas, E12.5–18.5 fetal livers and perinatal bone marrow. LSK cells are enriched with HSPCs[17–20] and share comparable phenotypes among all the examined tissues (Fig. 1a, Extended Data Fig. 1a and Supplementary Fig. 1). Treatment with Eto resulted in a greater number of DNA breaks in the HSPCs of early fetal livers (E12.5–14.5) than in the HSPCs of E12.5 placentas, late fetal livers (E15.5–18.5) and perinatal bone marrow. This was determined using DNA comet assays (Fig. 1b,c). Consistent results were obtained with the γ-H2AX immunofluorescence assay, which detects a protein that responds quickly to DNA breaks. Early fetal liver HSPCs showed more severe DNA damage than other tissues (Extended Data Fig. 1b,c). In an ex vivo experiment, exposure of HSPCs to 500 J of UV induced DNA breaks, with early fetal liver HSPCs exhibiting greater sensitivity to UV than other developing tissues (Extended Data Fig. 1d,e).

LSK cells were then flow sorted into three fractions based on slam gene expression: long-term haematopoietic stem cells (LT-HSCs), short-term HSCs (ST-HSCs) and multiple-potent progenitors (MPPs; Extended Data Fig. 2a and Supplementary Fig. 1). The sensitivity of these cell fractions to genotoxic agents changed with development. Eto treatment induced more DNA breaks in all three fractions of early fetal liver cells than in the other tissues, and the same trend was observed for the three cell fractions (Extended Data Fig. 2b,c). These ex vivo experimental results indicate that genome fragility varies when HSPCs migrate from the placenta to the fetal liver.

To investigate the effect in vivo, pregnant mice were intraperitoneally injected with Eto (5 mg kg^{-1}) on different embryonic days. At 1 h post-injection, the whole placenta or fetal liver was removed and stained with γ-H2AX and Kit antibodies in situ. Eto treatment caused DNA damages in placental and fetal liver cells including HSPCs (Kit^+) and non-HSPCs (Kit^-; Extended Data Fig. 2d). γ-$H2AX^+$ in Kit^+ cells are shown (Fig. 1d) and their proportions are summarized (Fig. 1e). Eto treatment induced more severe DNA damage in early fetal liver HSPCs at E12.5–14.5 than in E12.5 placental or late fetal liver HSPCs at E15.5–18.5 in vivo. A similar trend was observed in the HSC-enriched fraction when refined immunofluorescence assays were performed using additional markers ($CD150^+Lin^-CD41^-CD48^-$) in situ. Eto treatment induced DNA damage more easily in HSCs in the early fetal liver (Extended Data Fig. 2e,f). These results are consistent with those ex vivo, albeit a possibility of the non-direct effect on HSPCs in vivo.

Given that fetal HSPCs enriched by either LSK or more specific markers consistently exhibit sensitivity to genotoxins both ex vivo and in vivo, HSPCs are referred to as LSK enrichment unless further specified in the paper.

Pregnant mice at E12.5 or E16.5 were exposed to Eto treatment and observed until their offspring were delivered. The goal was to determine whether the treatment resulted in different phenotypical, functional, chromosomal and leukaemia-vulnerable alterations in HSPCs. These alterations could be detected postnatally after the HSPCs migrated into the bone marrow (Fig. 1f). The proportion of LSK populations was greater in the mice treated with Eto at E12.5 than in the mice treated at E16.5 and the untreated group (Fig. 1g,h). In addition, these cells exhibited stronger colony formation ability, as determined by a colony-forming cell assay (Fig. 1i,j). Whole-genome sequencing and chromosome fluorescence in situ hybridization revealed that 3-week-old bone marrow HSPCs treated with Eto at E12.5 carried more mutations than those treated at E16.5 (Extended Data Fig. 3).

Subsequently, the offspring of mice treated with Eto at E12.5 or E16.5 was exposed to the mutagenic agent *N*-ethyl-*N*-nitrosourea at 3 weeks of age to assess their differential vulnerability to leukaemic induction (Extended Data Fig. 4a). The occurrence of leukaemia was assessed through daily observation of leukaemic symptoms and signs, such as white toes, swollen lymph nodes and loss of body weight. In addition, weekly measurements of leukaemic-like cells were conducted through Giemsa staining of peripheral blood smears. Once these symptoms appeared (Fig. 1k and Extended Data Fig. 4b,c), the animals were euthanized, and the presence of leukaemia was confirmed by observing enlarged spleens and lymph nodes (Extended Data Fig. 4d), increased proportions of immature Lin^- cells in the bone marrow (Extended Data Fig. 4e) and definitive leukaemic cell infiltration in the bone marrow and spleen (Fig. 1l and Extended Data Fig. 4f). The latency period of induced leukaemia was significantly shorter in Eto-treated mice at E12.5 than in treated mice at E16.5 or untreated mice (Fig. 1m).

In conclusion, HSPCs in the early fetal liver exhibit the greatest susceptibility to genotoxic stresses, leading to a remarkably unstable genome.

HSPCs lack hepatocyte refuge in the early fetal liver

The selection of fetal livers as the primary site for haematopoiesis among developmental organs suggests that hepatocytes have a crucial role in HSPC maintenance, including maintaining genome integrity. Starting at E9.5, hepatocytes express albumin (Alb)[21]. To track hepatocyte development, Alb-Cre;ROSA26-LSL-tdTomato mice were used (Fig. 2a,b). By lineage tracing, we observed the relative cellular density and dynamics between hepatocytes and HSPCs (Kit^+). In the early fetal liver, HSPCs make up the majority of cells with a small number of hepatocytes. However, HSPCs gradually decrease in number and become surrounded by expanding hepatocytes (Fig. 2c). This finding suggested that hepatocyte development lags behind HSPC development in the fetal liver. On the basis of this observation and the high susceptibility of the early fetal liver (E12.5–14.5) to genotoxic damage (Fig. 1), we hypothesized that hepatocytes are crucial for maintaining genomic stability in HSPCs. To test this hypothesis, we manipulated hepatocyte development in Alb-Cre;ROSA26-LSL-DTA mice (Fig. 2d). Compared with that in control *Alb-cre* mice, the number of hepatocytes in these mice decreased by approximately 50% at E16.5 (Fig. 2e,g). The number of HSPCs (Kit^+) was reduced by 30% (Fig. 2f,h), whereas the density and distribution of arterial ($Sca\text{-}1^+$) and sinusoid ($CD144^+$) endothelial cells and pericytes ($Nestin^+$) were not significantly altered[22–24] (Fig. 2f,i–k). Eto treatment (5 mg kg^{-1}) resulted in more severe DNA damage in the HSPCs of Alb-Cre;ROSA26-LSL-DTA mice than in those of control mice (Fig. 2l,m). These results support a crucial role of hepatocytes in protecting HSPCs from genotoxic insults in the fetal liver, although more subtle modifications of other niche components, and thus indirect effects on HSPCs via their niche, cannot be fully ruled out. These results, together with those of the comparative functional assays across developmental stages (Fig. 1b–e) and of the lineage-tracing observation (Fig. 2a–c), also suggest that HSPCs lack the refuge of fully developed

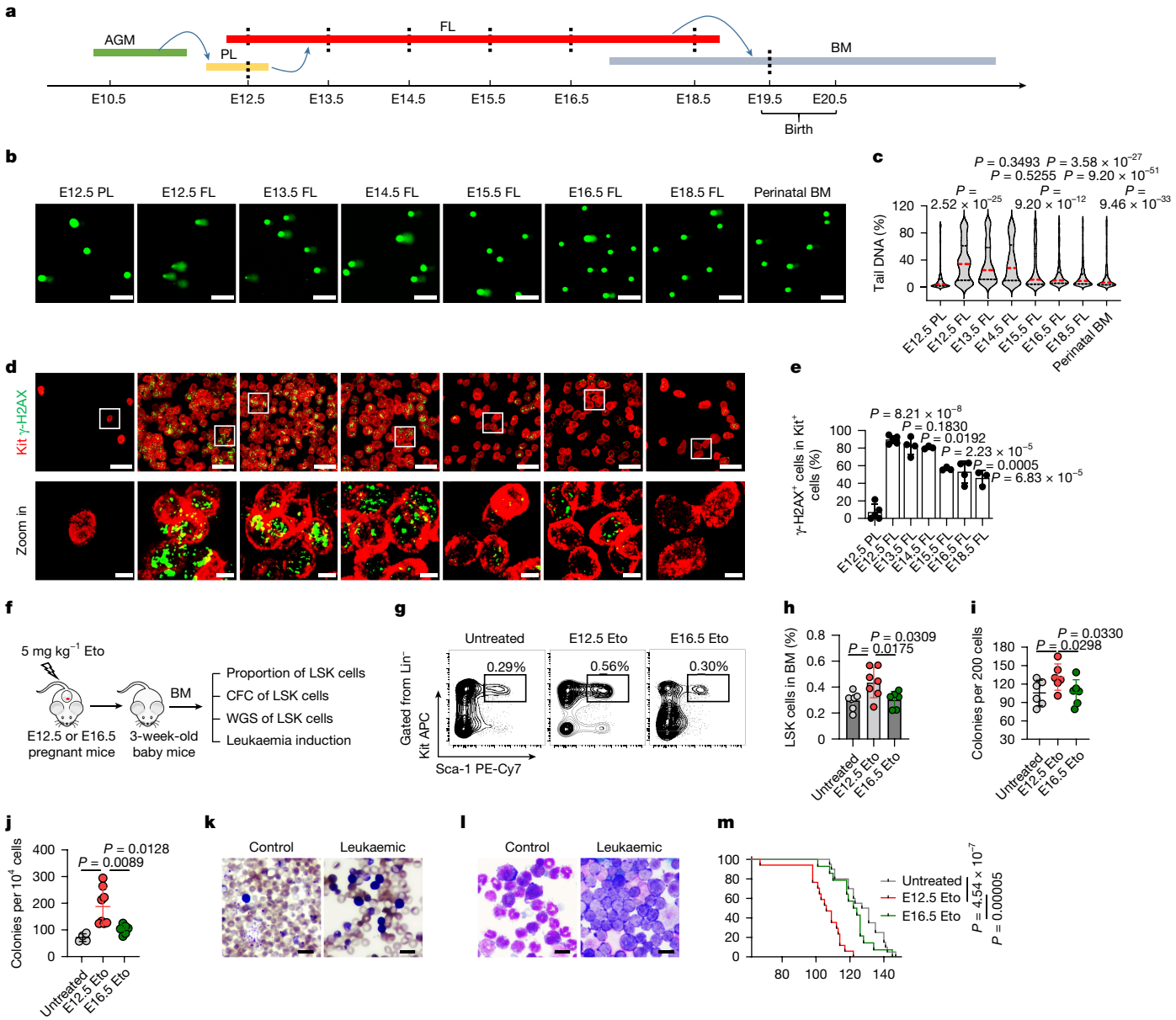

Fig. 1 | HSPC genomes are unstable in the early fetal liver. a, Mouse haematopoietic development and tissue harvesting of HSPCs (dashed lines) for the assessment of genome stability. AGM, aorta–gonad–mesonephros; BM, bone marrow; FL, fetal liver; PL, placenta. **b**,**c**, Representative comet-tail DNA images (**b**) and proportions (**c**) induced by etoposide (Eto) in HSPCs ($n = 3$). The medians (red dashed lines) and quartiles (black dashed lines) are shown. Scale bars, 50 µm. **d**,**e**, Representative in situ fluorescence images (**d**) and positive proportions (**e**) of γ-H2AX in Kit$^+$ HSPCs in whole-mount tissues after in vivo Eto treatment ($n = 5$ for the E12.5 placenta and E12.5 fetal liver; $n = 4$ for the E13.5 fetal liver and E16.5 fetal liver; and $n = 3$ for the E14.5 fetal liver, E15.5 fetal liver and E18.5 fetal liver). Scale bars, 30 µm and 5 µm. The white squares represent the areas enlarged in the bottom row. **f**, The assessment of alterations caused by Eto treatment. CFC, colony-forming cell; WGS, whole-genome sequencing. **g**,**h**, Representative flow cytometry images (**g**) and proportions (**h**) of 3-week-old bone marrow LSK cells ($n = 7$ for untreated and E12.5 Eto; and $n = 6$ for E16.5 Eto). **i**,**j**, Plating (**i**) and replating (**j**) CFC assays of 3-week-old bone marrow LSK cells ($n = 6$ per group (**i**); $n = 4$ for untreated, $n = 8$ for E12.5 Eto and $n = 6$ for E16.5 Eto (**j**)). **k**,**l**, Representative Giemsa-stained images of peripheral blood (**k**) and bone marrow (**l**) smears ($n = 7$ for control and $n = 31$ for leukaemic (**k**); $n = 7$ for control and $n = 13$ for leukaemic (**l**)). Scale bars, 100 µm. **m**, Onset of leukaemia induced in mice ($n = 20$ for untreated, $n = 17$ for E12.5 Eto and $n = 14$ for E16.5 Eto). The n represents independent experiments (**b**,**c**), individual fetuses (**d**,**e**), mice (**g**,**h**,**k**–**m**) and dishes (**i**,**j**) from three independent experiments. The mean ± s.d. is shown (**e**,**h**–**j**). Unpaired two-sided Student's t-test (**c**,**e**,**h**,**j**), unpaired one-sided Student's t-test (**i**) and log-rank (Mantel–Cox) test (**m**) were used.

hepatocytes in early fetal livers despite the limitations of our current depletion strategy (that is, possible effects earlier in development).

Hepatocytes secrete protective FetuA

To directly examine the effects of hepatocytes on the genomic protection of HSPCs and determine the underlying mechanism, we isolated Alb–tomato-positive hepatocytes from Alb-Cre;ROSA26-LSL-tdTomato mice at E12.5 or E16.5 (Fig. 3a). The purified hepatocytes were precultured in StemSpan medium supplemented with hepatocyte growth supplement, IL-6 and fetal bovine serum (SHIF) and then cultured in serum-free SHI medium[25,26]. E12.5 fetal liver HSPCs were then co-cultured in contact with hepatocytes or isolated from hepatocytes using a Transwell system that allows molecular factors to pass through. Genomic stability tests were subsequently conducted (Fig. 3a). Eto treatment resulted in significantly less DNA damage in HSPCs in

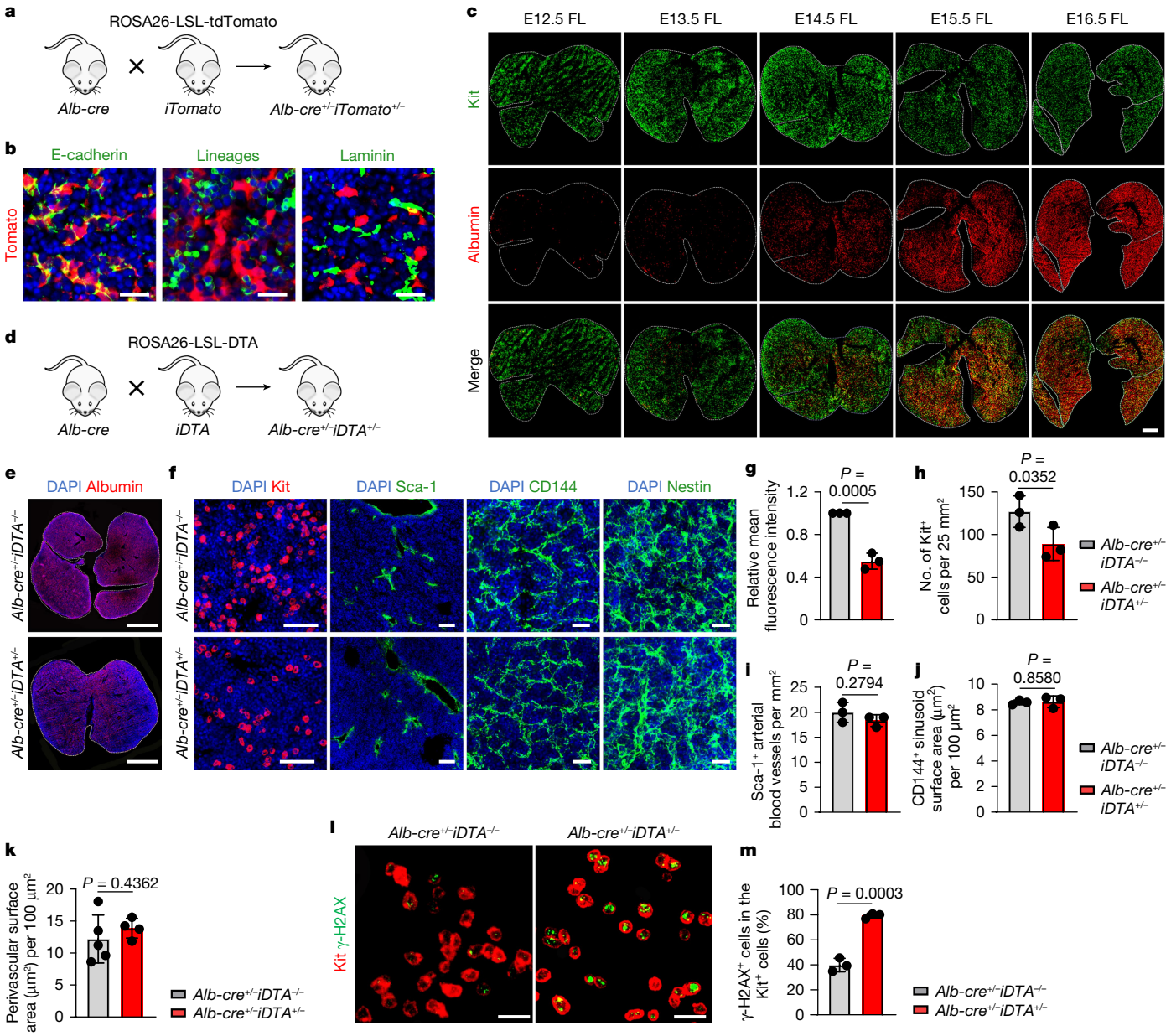

Fig. 2 | HSPCs lack hepatocyte refuge in the early fetal liver. a, The strategy of hepatocyte tracing using Alb-Cre;ROSA26-LSL-tdTomato mice. **b**, Alb-expressing cells (red) coexpressed the epithelial marker E-cadherin but not the haematopoietic cell lineage markers (CD3, B220, Gr-1, Mac-1 and Ter119) or the endothelial and mesenchymal marker laminin ($n = 3$). Scale bars, 25 μm. **c**, Representative fluorescence images showing tomato fluorescent protein-labelled hepatocytes and HSPCs (Kit (green)) in the developing fetal liver ($n = 3$). Scale bar, 500 μm. **d**, The strategy of hepatocyte depletion using Alb-Cre; ROSA26-LSL-DTA mice. **e**,**g**, Representative fluorescence images (**e**) and mean fluorescence intensity (**g**) of albumin red in the E16.5 fetal liver of *Alb-cre*$^{+/-}$*iDTA*$^{-/-}$ and *Alb-cre*$^{+/-}$*iDTA*$^{+/-}$ mice ($n = 3$). Scale bars, 1 mm. **f**,**h**–**k**, Representative fluorescence images (**f**) and the numbers of Kit$^+$ cells (**h**), the arterial blood vessels (Sca-1$^+$; **i**), the sinusoid surface area (CD144$^+$; **j**) and the perivascular surface area (Nestin$^+$; **k**) in the E16.5 fetal liver of *Alb-cre*$^{+/-}$*iDTA*$^{+/-}$ and *Alb-cre*$^{+/-}$*iDTA*$^{-/-}$ mice ($n = 3$; $n = 5$ for *Alb-cre*$^{+/-}$*iDTA*$^{-/-}$; $n = 4$ for *Alb-cre*$^{+/-}$*iDTA*$^{+/-}$ (**h**–**k**)). Scale bars, 25 μm and 100 μm. **l**,**m**, Representative fluorescence images (**l**) and positive cell proportions (**m**) of γ-H2AX in Kit$^+$ HSPCs in the E16.5 fetal liver from *Alb-cre*$^{+/-}$*iDTA*$^{+/-}$ and *Alb-cre*$^{+/-}$*iDTA*$^{-/-}$ mice after Eto treatment in vivo ($n = 3$). Scale bars, 20 μm. The *n* represents independent experiments (**b**,**c**) and individual fetuses from three independent experiments (**e**–**m**). The mean ± s.d. is shown (**g**–**k**,**m**). Unpaired one-sided Student's *t*-test (**h**) and unpaired two-sided Student's *t*-test (**g**,**i**–**k**,**m**) were used.

co-culture, either in contact with or isolated from hepatocytes, than in control cultures without hepatocytes (Fig. 3b,c). Similar results were obtained when co-culturing LT-HSCs, ST-HSCs and MPPs (Extended Data Fig. 5a,b). Therefore, fetal hepatocytes secrete paracrine factors that protect the HSPC genomes.

To identify the factors involved, the supernatant (conditioned medium (co-SHI)) was collected (Fig. 3a). Culturing of HSPCs in co-SHI, which were conditioned from either E12.5 or E16.5 hepatocytes, increased the resistance of HSPCs to Eto compared with that of HSPCs cultured in basic SHI medium (Extended Data Fig. 5c,d). These results further support that the lack of genomic protection in the early fetal liver is due to the relatively low number of hepatocytes compared with that of haematopoietic cells (Fig. 2c). E16.5 hepatocyte-conditioned co-SHI was used for the identification of genome-protective factors due to its greater availability. The SHI and co-SHI media were analysed by mass spectrometry. A total of 203 proteins were more enriched in co-SHI than in SHI (Fig. 3d). The proteomes of fetal liver tissues at E12.5 and E16.5 were also compared. Exactly 113 secretory proteins were lacking (fold change ≥ 2; $P < 0.05$) in E12.5 fetal livers compared with E16.5 fetal livers (Fig. 3d), and 22 secretory proteins were enriched in

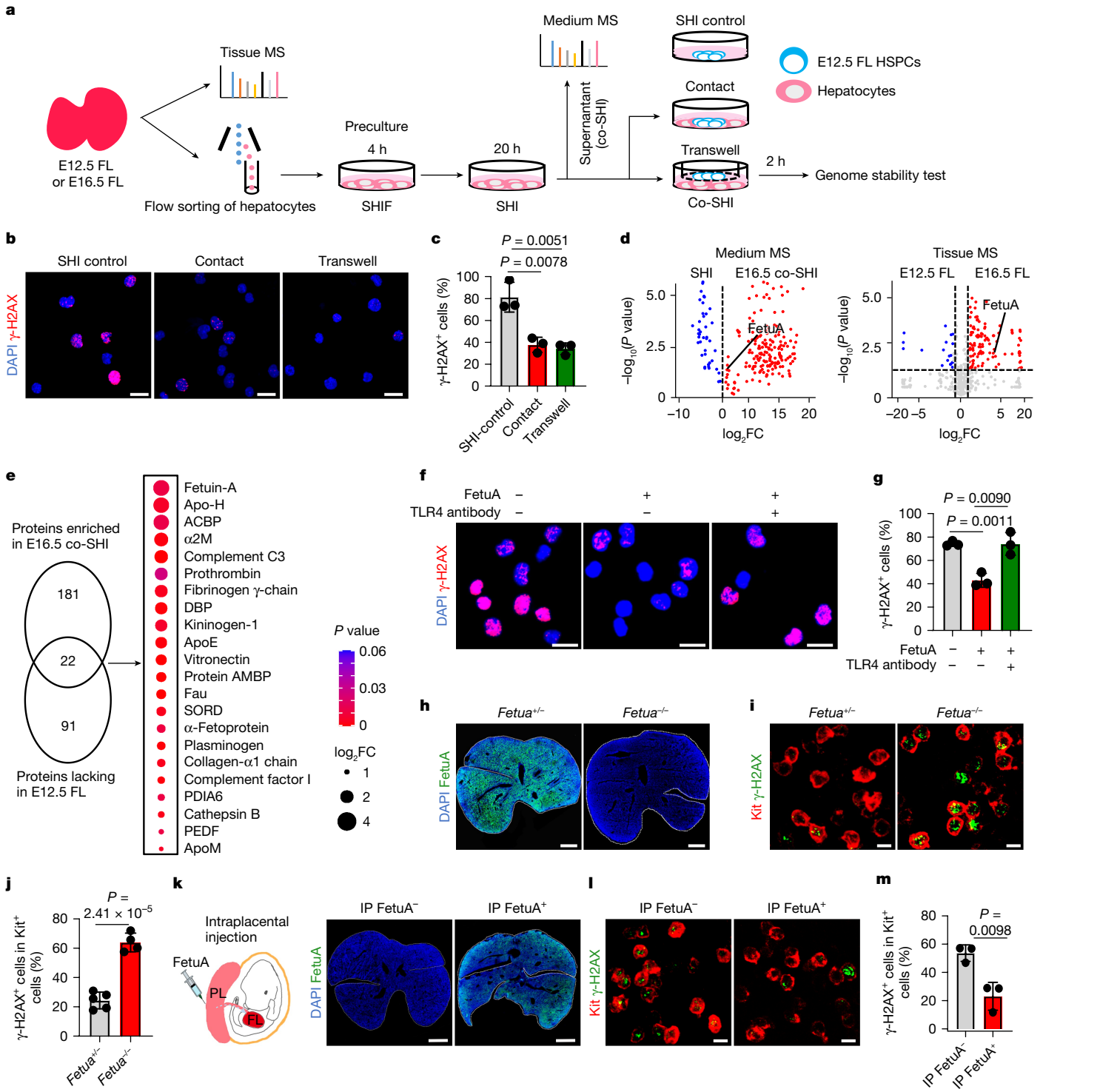

Fig. 3 | Hepatocyte-paracrine FetuA protects the HSPC genome. **a**, Mechanistic investigation of the effect of hepatocytes on HSPCs. SHIF, SHI and co-SHI are culture media (see Methods). MS, mass spectrometer. **b**,**c**, Representative fluorescence images (**b**) and positive proportions (**c**) of γ-H2AX Eto induced in E12.5 fetal liver HSPCs in culture ($n = 3$). Scale bars, 20 µm. **d**, Volcano plots showing proteins in the media ($n = 3$ for SHI and $n = 4$ for co-SHI) and secretory proteins in fetal liver tissues ($n = 4$). The vertical dashed lines indicate the fold change (FC) threshold ($\log_2FC = 0$, $\log_2FC > 1$ or $\log_2FC < -1$), and the horizontal dashed line indicates the P value threshold ($P = 0.05$). **e**, Venn diagram showing proteins enriched in E16.5 co-SHI and lacking in the E12.5 fetal liver (more than twofold change, $P < 0.05$). The bubble chart and colours show the fold change and P values for the comparison between the E12.5 and E16.5 fetal liver. **f**,**g**, Representative fluorescence images (**f**) and positive proportions (**g**) of γ-H2AX Eto induced in HSPCs with or without FetuA and TLR4 antibodies in culture ($n = 3$). Scale bars, 20 µm. **h**, Representative fluorescence images of FetuA in the E16.5 fetal liver of *Fetua*$^{+/-}$ or *Fetua*$^{-/-}$ mice. Scale bars, 500 µm. **i**,**j**, Representative fluorescence images (**i**) and positive proportions (**j**) of γ-H2AX in Kit$^+$ HSPCs in the E16.5 fetal liver Eto induced in *Fetua*$^{+/-}$ or *Fetua*$^{-/-}$ mice ($n = 5$ for *Fetua*$^{+/-}$ and $n = 4$ for *Fetua*$^{-/-}$). Scale bars, 10 µm. **k**–**m**, Representative fluorescence images of FetuA (**k**) or γ-H2AX (**l**) and its positive proportions (**m**) in Kit$^+$ HSPCs in the E16.5 fetal liver Eto induced in *Fetua*$^{-/-}$ mice with or without FetuA ($n = 3$). Scale bars, 500 µm (**k**) and 10 µm (**l**). IP, intraplacental. The n represents individual samples (**b**–**g**) and fetuses (**h**–**m**) from three (**b**,**c**,**f**–**m**) or four (**d**) independent experiments. The mean ± s.d. is shown (**c**,**g**,**j**,**m**). Unpaired two-sided Student's t-test (**c**–**e**,**g**,**j**,**m**) was used.

co-SHI (Fig. 3e). FetuA was identified among the significantly altered proteins. The presence and concentration of FetuA in the medium and fetal liver tissues were confirmed (Extended Data Fig. 5e,f and Supplementary Fig. 2). Double immunofluorescence stainings showed the presence of FetuA inside hepatocytes (E-cadherin$^+$) and absence inside haematopoietic (CD45$^+$ or Ter119$^+$), endothelial (Scal-1$^+$ or CD144$^+$) and mesenchymal (Nestin$^+$) cells (Extended Data Fig. 5g). Hence, FetuA is primarily expressed by hepatocytes and so is commonly considered as a hepatokine[15,16]. FetuA colocalized on the cell surface of HSPCs (CD150$^+$) in the E16.5 fetal liver in situ, indicating that hepatocytes support HSPCs through a paracrine mechanism (Extended Data Fig. 5h). Recombinant FetuA was used to treat E12.5 fetal liver HSPCs in culture, and the resulting HSPCs became more tolerant of Eto (Fig. 3f,g and Extended Data Fig. 5i,j).

To further confirm the genome-protective role of FetuA in the fetal liver and perinatal bone marrow, we treated *Fetua*-knockout (FKO) mice (Fig. 3h and Extended Data Fig. 5k) with 5 mg kg^{-1} Eto at E16.5 or at E19. HSPCs from *Fetua*$^{-/-}$ mice were more sensitive to genotoxins than those from *Fetua*$^{+/-}$ mice, confirming the protective role of FetuA in the fetal liver (Fig. 3i,j) and perinatal bone marrow (Extended Data Fig. 5l,m).

Finally, we investigated whether the lack of HSPC genomic protection from hepatocytes in mice at the early fetal liver developmental stage, in FKO mice and in Alb-Cre;ROSA26-LSL-DTA mice could be remedied in vivo. Recombinant FetuA was administered via intraplacental injection. At 2 h post-injection, the concentration of FetuA in the fetal liver increased (Fig. 3k and Extended Data Fig. 5n,q). Eto treatment (5 mg kg^{-1}) induced less DNA damage to HSPCs in FetuA-treated fetuses than in untreated fetuses (Fig. 3l,m and Extended Data Fig. 5o,p,r,s). Hence, the HSPC genome was protected from genotoxic attack by FetuA administration in vivo.

In conclusion, the hepatocyte paracrine FetuA provides HSPCs with genomic protection from genotoxic stresses in the fetal liver, although a contribution of FetuA from cells other than hepatocytes cannot be excluded in the absence of tissue-specific deletion of FetuA.

FetuA activates TLR4 to reduce the R-loop

Toll-like receptor 4 (TLR4) serves as the receptor for FetuA[27]. The protective effects of FetuA on the HSPC genome were nullified by a neutralizing antibody to TLR4 (Fig. 3f,g). The colocalization of FetuA with TLR4 was observed on the surface of cultured HSPCs (Fig. 4a). Upon FetuA treatment, the colocalization and polarization of TLR4 and MYD88 in the cell membrane indicated the formation of a FetuA–TLR4–MYD88 complex and the potential activation of their downstream pathway[28] (Fig. 4b). Furthermore, FetuA treatment led to an increase in the expression of basic leucine zippers (bZIPs; Jun, JunB and Fosl1) and phosphorylated bZIPs in HSPCs, as confirmed by western blotting (Fig. 4c and Supplementary Fig. 2).

To investigate the mechanism by which the FetuA-activated TLR4–MYD88–bZIP pathway provides protection to the HSPC genome, we conducted a comparative analysis of the chromatin state and corresponding transcriptome in E12.5 fetal liver HSPCs with or without FetuA treatment. This was achieved through assay for transpose-accessible chromatin using sequencing (ATAC-seq) and RNA-seq. The acquired ATAC-seq data exhibited consistency among the three replicates in each group (Extended Data Fig. 6a). The accessible chromatin in the nucleosome-free and nucleosome-associated regions was readily discernible for further analysis (Extended Data Fig. 6b). The differential opening and closing peaks are depicted (Fig. 4d). Of note, the opening regions post-FetuA treatment exhibited an enrichment of bZIP motifs (Fig. 4e), which aligns with the increase in protein expression and phosphorylation (Fig. 4c). bZIP motifs were enriched in genes involved in the regulation of R-loop formation, such as the helicase *Blm*, *Fanci* and *Smarcc1* (Fig. 4d and Extended Data Fig. 6c), and these genes exhibited transcriptional upregulation[3,29–31] (Fig. 4f). Furthermore, the binding of the transcription factor bZIPs to the *Blm* gene was identified by Cut&Tag for Jun, JunB and Fosl1 (Extended Data Fig. 6d,e). To further validate the regulatory effect of FetuA on *Blm* expression through bZIPs, a series of biochemical experiments was performed. BLM protein expression was much lower in E12.5 fetal liver HSPCs than in E16.5 HSPCs (Extended Data Fig. 6f and Supplementary Fig. 2). FetuA-treatment promoted *Blm* expression in both LSK-enriched and Lin$^-$-enriched E12.5 fetal liver HSPCs (Fig. 4c,g, Extended Data Fig. 6g,h and Supplementary Fig. 2), and this promotional effect was nullified by a specific bZIP inhibitor, SR11032 (Fig. 4g and Supplementary Fig. 2), indicating that FetuA regulates *Blm* expression by activating the TLR4–bZIP pathway; however, nonspecific effects of the inhibitor cannot be fully ruled out.

These findings suggest that the accumulation of R-loops is a contributing factor to the increased chromosome fragility in early fetal liver HSPCs. In addition, our study suggested that the FetuA-activated pathway acts as a mechanism to protect the genome by interfering with the formation or removal of R-loops. To support this hypothesis, we conducted an immunofluorescence assay using dRNH1 or 2×HBD antibodies, which specifically bind to DNA-RNA hybrids[32,33]. We observed a stronger signal in E12.5 fetal liver HSPCs than in the E12.5 placenta and E16.5 fetal liver HSPCs (Extended Data Fig. 7a–d). Furthermore, the dRNH1 signal in E12.5 fetal liver HSPCs was significantly reduced after FetuA treatment (Fig. 4h,i). The specific inhibitor ML216, which targets the BLM helicase, reversed the removal effect of FetuA on R-loops (Fig. 4h,i) and the protective effects on the HSPC genome (Fig. 4j,k). These results demonstrated that FetuA regulates BLM to resolve R-loops and to protect the HSPC genome; however, the nonspecific effects of the inhibitor cannot be fully excluded.

Moreover, when we evaluated more enriched LT-HSCs, ST-HSCs and MPPs, the dRNH1 signal was stronger in all three populations of E12.5 fetal livers than in E16.5 fetal livers (Extended Data Fig. 7e,f), and the signal in E12.5 fetal liver cells was reduced after FetuA treatment (Extended Data Fig. 7g,h).

Together, our results demonstrate that FetuA protects the HSPC genome by activating the TLR4–bZIP–BLM cascade to prevent R-loop accumulation (Fig. 4l).

Replication and transcription in HSPCs

Considering that pathogenetic R-loops are possibly formed by collisions between DNA replication and gene transcription, we conducted comparative analyses of the cell cycle status of HSPCs between E12.5 placentas and E12.5 and E16.5 fetal livers. The results showed that a larger proportion of HSPCs remained in a quiescent state (G0 stage) in the placenta, whereas most of the HSPCs quickly entered the cell cycle upon migration into the fetal liver, as evidenced by DNA–Hoechst and RNA–pyronin Y staining ex vivo (Extended Data Fig. 8a,b). Furthermore, the majority of HSPCs in fetal livers were in the S stage, as indicated by the incorporation of synthetic DNA de novo labelled with 5-ethynyl-2′-deoxyuridine in vivo and measured by flow cytometry (Extended Data Fig. 8c,d). Consistent dynamics were observed in each fraction of LT-HSCs, ST-HSCs and MPPs when analysing the three fractions within LSK cells in the cell cycle (Extended Data Fig. 8e,f). These results suggest that an increased proportion of HSPCs undergo expansion and DNA replication after migrating into the fetal liver.

Moreover, we performed ethyluridine incorporation experiments to label synthetic RNA de novo. The results revealed a significantly greater proportion of ethyluridine-positive HSPCs in the fetal liver than in the placenta, indicating an increased proportion of HSPCs undergoing gene transcription in the fetal liver (Extended Data Fig. 8g,h).

Simultaneous DNA replication and gene transcription in fetal liver HSPCs may lead to an increase in collisions. An immunofluorescence assay for phosphorylated RPA (p-RPA), which is a marker for stalled replication caused by replication–transcription collisions, revealed

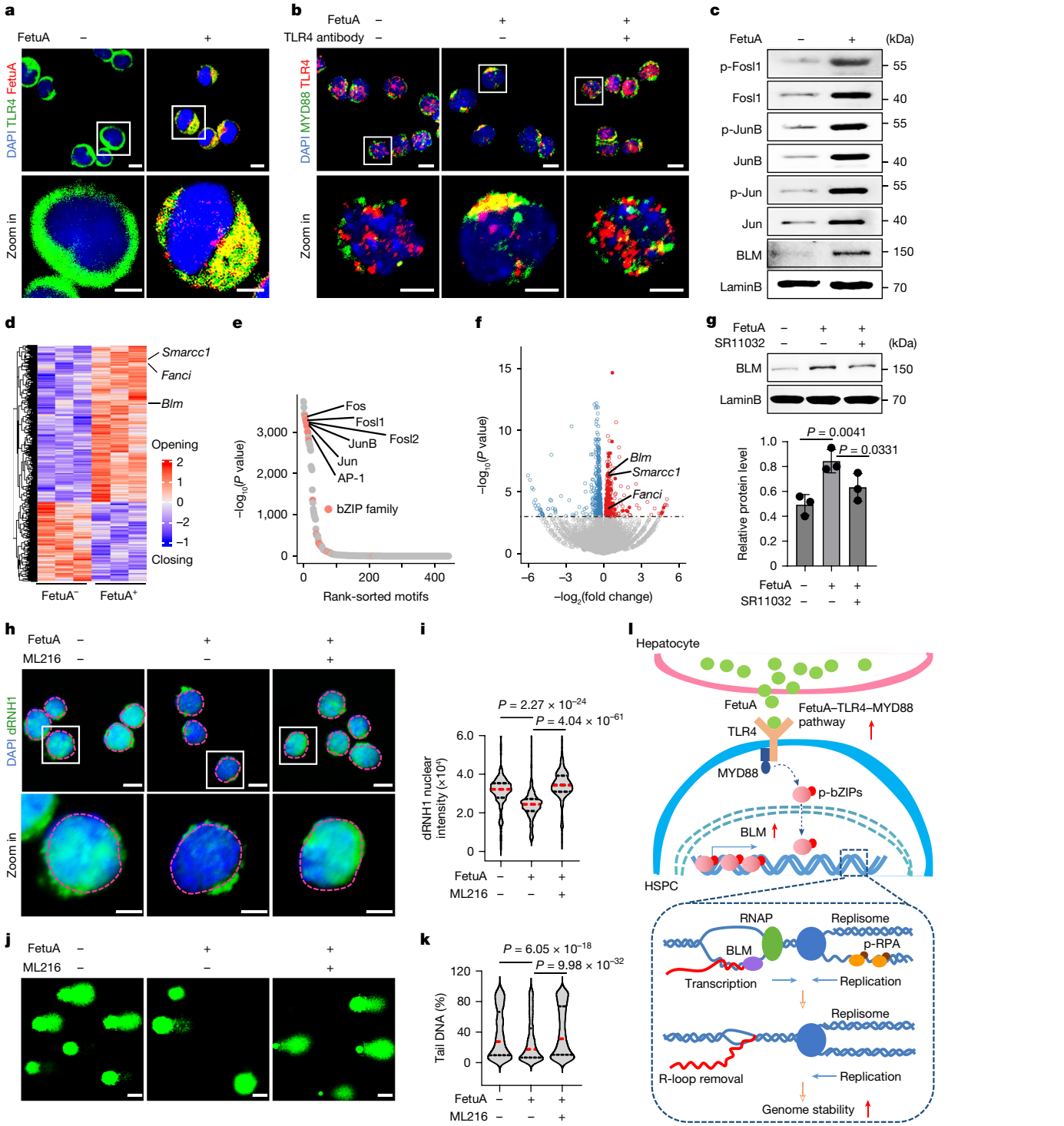

Fig. 4 | FetuA activates the TLR4 pathway to prevent R-loop accumulation. **a**, Representative fluorescence images of FetuA and TLR4 on E12.5 fetal liver HSPCs with or without FetuA treatment. Scale bars, 10 μm and 5 μm. The white squares represent the areas enlarged in the bottom row. **b**, Representative fluorescence images of TLR4 and MYD88 on HSPCs cultured with or without FetuA and TLR4 antibodies. Scale bars, 10 μm and 5 μm. **c**, Western blots of bZIPs (Fosl1, JunB and Jun), their phosphorylated (p) forms and BLM in E12.5 fetal liver HSPCs cultured with or without FetuA. **d**, ATAC-seq analysis of E12.5 fetal liver HSPCs with or without FetuA treatment, showing the differential opening and closing peaks and R-loop regulatory genes *Smarcc1*, *Fanci* and *Blm*. **e**, DNA-binding factors whose motifs were enriched in the opening regions of panel **d**. **f**, Volcano plot showing the differential gene expression. The horizontal dashed line shows the *P* value threshold ($P = 0.05$). The blue and red spots show the downregulated or upregulated genes, respectively, in FetuA-cultured HSPCs. **g**, Western blots (top) and signal intensity (bottom) of BLM in E12.5 fetal liver Lin⁻ HSPCs cultured with or without FetuA and the bZIP inhibitor SR11032 (data shown as mean ± s.d.). **h**,**i**, Representative fluorescence images (**h**) and nuclear signal intensity (**i**) of dRNH1 in E12.5 fetal liver HSPCs cultured with or without FetuA and the BLM inhibitor ML216. The nuclear regions are circled by dotted lines. Scale bars, 10 μm and 5 μm. **j**,**k**, Representative comet-tail DNA images (**j**) and percentages (**k**) of Eto induced in E12.5 fetal liver HSPCs cultured with or without FetuA and the BLM inhibitor ML216. Scale bars, 20 μm. **l**, A working model of the FetuA–TLR4 pathway in protecting the HSPC genome. RPA, replication protein A; RNAP, RNA polymerase. $n = 3$ independent experiments (**a**–**k**). The medians (red dashed lines) and quartiles (black dashed lines) are shown (**i**,**k**). Two-sided binomial test (**e**), two-sided Wald test (**f**), unpaired one-sided Student's *t*-test (**g**) and unpaired two-sided Student's *t*-test (**i**,**k**) were used.

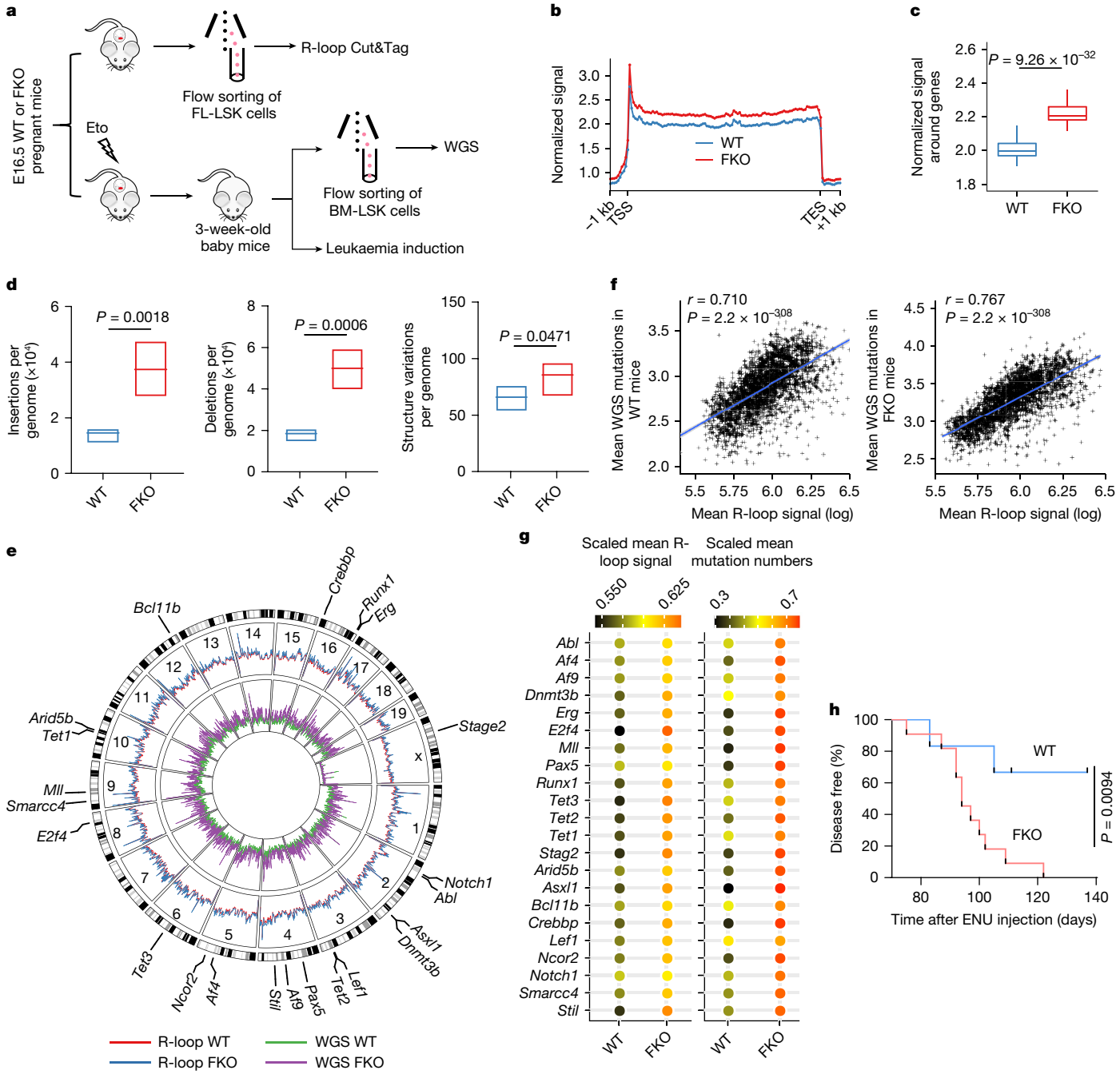

Fig. 5 | A lack of FetuA increased vulnerability to leukaemogenesis. **a**, Experimental design for genome-wide R-loop sequencing (R-loop Cut&Tag), whole-genome sequencing (WGS) and leukaemia induction. **b**, Gene metaplots analysis of R-loop Cut&Tag. The mean coverages of R-loop signals over gene bodies (±1 kb) in E16.5 fetal liver HSPCs from WT and FKO mice are shown ($n = 3$). TSS, transcription start site; TES, transcription end site. **c**, Boxplots showing the R-loop signal over gene bodies (±1 kb) in E16.5 fetal liver HSPCs from WT and FKO mice ($n = 3$). The boxes delimit the lower (25th) and upper (75th) interquartile, and the horizontal line represents the median. **d**, The number of chromosomal insertions (left), deletions (middle) and structural variations (right) per genome in bone marrow HSPCs from 3-week-old Eto-treated WT and FKO mice at E16.5 ($n = 4$). The boxes delimit the minima and maxima, and the horizontal line represents the mean. **e**, Circos plots showing the genome-wide distribution of the identified R-loop events (outer circles; $n = 3$ per group) and mutations (inner circles; $n = 4$ per group) in HSPCs from WT and FKO mice. **f**, Dot plots revealing the correlation between R-loop signals and mutations in WT (left) and FKO (right) mice ($n = 3$ for R-loop and $n = 4$ for WGS). **g**, Mean R-loop signal ($n = 3$) and mutation numbers ($n = 4$) of the genes frequently involved in leukaemia in HSPCs from WT and FKO mice. **h**, The onset of leukaemia induced in WT and FKO mice by Eto treatment at E16.5 and *N*-ethyl-*N*-nitrosourea (ENU) treatment at 3 weeks of age (see Extended Data Fig. 4a; $n = 6$ for WT and $n = 11$ for FKO). The n represents individual samples (**b**–**g**) and mice (**h**) from three independent experiments. Two-sided Wilcoxon test (**c**), unpaired two-sided Student's t-test (**d**), two-sided Pearson test (**f**) and log-rank (Mantel–Cox) test (**h**) were used.

that the signal significantly increased in HSPCs in E12.5 fetal livers compared with E12.5 placentas and then decreased again in E16.5 fetal livers (Extended Data Fig. 8i,j). In addition, the p-RPA signal decreased in E12.5 fetal liver HSPCs after FetuA treatment (Extended Data Fig. 8k,l). Therefore, the dynamics of the p-RPA signal were consistent with the changes in R-loop accumulation and genome instability (Fig. 4h–k). However, treatment with FetuA and the BLM inhibitor ML216 did not have a significant effect on the cell cycle of E12.5 fetal liver HSPCs

(Extended Data Fig. 8m,n), indicating that FetuA did not protect HSPC genomes by affecting their cell cycle; however, potential off-target effects of the inhibitor cannot be excluded.

In summary, fetal liver HSPCs experience simultaneous DNA replication and gene transcription, leading to increased replication–transcription conflicts, R-loop accumulation and subsequent genomic instability until they receive sufficient genomic protection from the hepatocyte-paracrine FetuA in the fetal liver (Fig. 4l).

Lack of FetuA results in leukaemogenesis

Having established the protective effect of FetuA in reducing R-loop accumulation in HSPC genomes (Figs. 3 and 4), we performed genome-wide R-loop sequencing (Cut&Tag for R-loop) to investigate whether the R-loops enriched in haematopoietic regulatory genes are involved in leukaemogenic mutations[34] (Extended Data Fig. 9a). The genomic distribution of R-loop peaks in each cell type and their enrichment in various types of repetitive elements indicated that the data were qualified for further analysis[35,36] (Extended Data Fig. 9b,c). Gene metaplots analysis demonstrated greater R-loop enrichment in gene bodies in the E12.5 fetal liver than in the E12.5 placenta and E16.5 fetal liver (Extended Data Fig. 9d,e), which is consistent with the results of dRNH1 and 2×HBD immunofluorescence (Extended Data Fig. 7a–d). Gene Ontology analysis of differentially annotated peak genes revealed that the differential R-loop accumulation peaks in the E12.5 fetal liver compared with the E12.5 placenta and E16.5 fetal liver were associated with DNA replication (cell proliferation), gene transcription and developmental haematopoiesis (Extended Data Fig. 9f), particularly with genes frequently implicated in leukaemogenesis[37–40] (Extended Data Fig. 9g). Consistently, after FetuA treatment, the overall R-loop signal was reduced (Extended Data Fig. 9h,i), and less R-loop accumulation was observed in the regulatory gene regions involved in haematopoiesis (Extended Data Fig. 9f,g).

To further determine the effect of FetuA on R-loop accumulation and mutagenesis, we conducted genome-wide R-loop sequencing and whole-genome sequencing in HSPCs from FKO mice and control wild-type (WT) mice (Fig. 5a). As expected, R-loop accumulation (Fig. 5b,c) and mutation numbers (Fig. 5d) were significantly greater in FKO mice than in WT mice. The circus plots displayed the genome-wide distribution of identified R-loop events and mutations (Fig. 5e). The distribution of R-loops was positively correlated with mutations in both the presence and the absence of FetuA (Fig. 5f). Moreover, we observed that numerous important haematopoietic regulatory genes were located in these R-loop-enriched and highly mutated regions (Fig. 5g). These findings suggest that the absence of FetuA protection may lead to vulnerability to leukaemogenesis. When comparing the oncogenesis of leukaemia induced by Eto treatment at E16.5 and *N*-ethyl-*N*-nitrosourea treatment postnatally in WT and FKO mice, we found that the latency to induced leukaemia was significantly shorter in FKO mice than in WT mice (Fig. 5h).

In summary, FetuA is essential for maintaining genome stability of fetal HSPCs, and a lack of FetuA increases susceptibility to mutagenesis and leukaemogenesis.

Similar protective mechanism in humans

Human samples were examined to determine the conservation between mice and humans (Extended Data Fig. 10a,b). Eto treatment caused more DNA damage in HSPCs (Lin^- and $CD34^+$)[41] from the early fetal liver of the first trimester (embryonic weeks 7–10 (E7–10w)) than in HSPCs from the later fetal liver of the second trimester (E11–19w) or neonatal cord blood (Extended Data Fig. 10c,d). Similarly, human HSPCs in the early fetal liver were more susceptible to genotoxic insult than those in the later fetal liver or cord blood, consistent with findings in mice.

The FetuA concentration in the fetal liver of the first trimester was considerably lower than that in the fetal liver of the second trimester (Extended Data Fig. 10e,f). $CD34^+$ HSPCs were surrounded and bound by FetuA in the fetal liver at E13w but not at E7w (Extended Data Fig. 10g). Ex vivo Eto treatment induced less DNA damage in HSPCs in the presence of FetuA than in the absence of FetuA (Extended Data Fig. 10h). Furthermore, FetuA interacted with TLR4 on the surface of HSPCs (Extended Data Fig. 10i). These findings provide further confirmation that hepatocytes provide genome protection to HSPCs through a paracrine mechanism, and this protection is lacking in the fetal liver of early humans, similar to the fetal liver of mice.

Finally, the concentration of FetuA in the bone marrow blood sera of infant patients with leukaemia and benign samples of patients with non-leukaemia was measured. The concentration of FetuA was significantly lower in leukaemic sera than in non-leukaemic sera (Extended Data Fig. 10j), indicating that the absence of FetuA protection is a risk factor for childhood leukaemia.

Overall, we observed a similar genome-protective mechanism in humans as that previously identified in mice. The lack of this protection is correlated with the onset of childhood leukaemia.

Discussion

During embryonic development, there is a significant expansion of highly proliferative cells in the three germinal layers to produce a wide range of functional cell types and form tissues and organs. It is a considerable challenge to maintain genomic integrity in these tissue-forming cells during DNA replication and normal cellular activity with specific gene transcription. However, further studies are needed to uncover the mechanisms by which developmental organ tissues provide genome protection for tissue-forming cells and how the absence or pathological loss of this protection leads to DNA damage and genome instability in the presence of endogenous (for example, metabolic) or exogenous genotoxic agents. In this study, we discovered a genome-protective mechanism in the fetal liver: hepatocyte-paracrine FetuA protects the HSPC genome by preventing R-loop accumulation. We also found that this genome-protective mechanism is absent in the early fetal liver due to the delayed development of hepatocytes, which exposes newly colonized HSPCs to genotoxic insults in unprotected environments lacking the hepatocyte-paracrine factor FetuA. Within this specific time period, HSPCs become highly susceptible to genotoxic insults. In pathological processes, this unprotected time window is either extended or protection is lost, leading to persistent DNA damage and genome instability throughout the developmental stage and postnatal period, thereby facilitating the initiation and accumulation of mutations during this prolonged genome-unstable period.

Therefore, the findings of this study will have implications in the following: (1) mechanical revelation of the establishment of genetic and epigenetic homeostasis during development; (2) identification of developmental features that are vulnerable to development-related diseases; and (3) exploitation of effective approaches to prevent these diseases. Further studies are required to determine whether such a mechanism is universal or an analogous mechanism that also appears in other developmental organs or tissues and to screen out the druggable substitutes of FetuA or the agonists or antagonists of its activated pathway for the prevention of development-related diseases, such as childhood cancer.

Online content

Any methods, additional references, Nature Portfolio reporting summaries, source data, extended data, supplementary information, acknowledgements, peer review information; details of author contributions and competing interests; and statements of data and code availability are available at https://doi.org/10.1038/s41586-024-08307-x.

1. Saxena, S. & Zou, L. Hallmarks of DNA replication stress. *Mol. Cell* **82**, 2298–2314 (2022).
2. Gaillard, H. & Aguilera, A. Transcription as a threat to genome integrity. *Annu. Rev. Biochem.* **85**, 291–317 (2016).
3. Aguilera, A. & Garcia-Muse, T. Causes of genome instability. *Annu. Rev. Genet.* **47**, 1–32 (2013).
4. Hoeijmakers, J. H. Genome maintenance mechanisms for preventing cancer. *Nature* **411**, 366–374 (2001).
5. Branzei, D. & Foiani, M. Maintaining genome stability at the replication fork. *Nat. Rev. Mol. Cell Biol.* **11**, 208–219 (2010).
6. Dion, V. & Gasser, S. M. Chromatin movement in the maintenance of genome stability. *Cell* **152**, 1355–1364 (2013).
7. Papamichos-Chronakis, M. & Peterson, C. L. Chromatin and the genome integrity network. *Nat. Rev. Genet.* **14**, 62–75 (2013).
8. Crawford, L. W., Foley, J. F. & Elmore, S. A. Histology atlas of the developing mouse hepatobiliary system with emphasis on embryonic days 9.5–18.5. *Toxicol. Pathol.* **38**, 872–906 (2010).
9. Liu, C. et al. Delineating spatiotemporal and hierarchical development of human fetal innate lymphoid cells. *Cell Res.* **31**, 1106–1122 (2021).
10. Gao, S. et al. Identification of HSC/MPP expansion units in fetal liver by single-cell spatiotemporal transcriptomics. *Cell Res.* **32**, 38–53 (2021).
11. Ober, E. A. & Lemaigre, F. P. Development of the liver: insights into organ and tissue morphogenesis. *J. Hepatol.* **68**, 1049–1062 (2018).
12. Mikkola, H. K. & Orkin, S. H. The journey of developing hematopoietic stem cells. *Development* **133**, 3733–3744 (2006).
13. Chou, S. & Lodish, H. F. Fetal liver hepatic progenitors are supportive stromal cells for hematopoietic stem cells. *Proc. Natl Acad. Sci. USA* **107**, 7799–7804 (2010).
14. Kamiya, A. et al. Fetal liver development requires a paracrine action of oncostatin M through the gp130 signal transducer. *EMBO J.* **18**, 2127–2136 (1999).
15. Jirak, P. et al. Clinical implications of fetuin-A. *Adv. Clini. Chem.* **89**, 79–130 (2019).
16. Icer, M. A. & Yıldıran, H. Effects of nutritional status on serum fetuin-A level. *Crit. Rev. Food Sci. Nutr.* **60**, 1938–1946 (2019).
17. Okada, S. et al. In vivo and in vitro stem cell function of c-Kit- and Sca-1-positive murine hematopoietic cells. *Blood* **80**, 3044–3050 (1992).
18. Morrison, S. J., Hemmati, H. D., Wandycz, A. M. & Weissman, I. L. The purification and characterization of fetal liver hematopoietic stem cells. *Proc. Natl Acad. Sci. USA* **92**, 10302–10306 (1995).
19. Ottersbach, K. & Dzierzak, E. The murine placenta contains hematopoietic stem cells within the vascular labyrinth region. *Dev. Cell* **8**, 377–387 (2005).
20. Guo, X. L. et al. Recipient bone marrow assimilates the myeloid/lymphoid reconstitution of distinct fetal hematopoietic stem cells. *Oncotarget* **8**, 108981–108988 (2017).
21. Miyajima, A., Tanaka, M. & Itoh, T. Stem/progenitor cells in liver development, homeostasis, regeneration, and reprogramming. *Cell Stem Cell* **14**, 561–574 (2014).
22. Khan, J. A. et al. Fetal liver hematopoietic stem cell niches associate with portal vessels. *Science* **351**, 176–180 (2016).
23. Itkin, T. et al. Distinct bone marrow blood vessels differentially regulate haematopoiesis. *Nature* **532**, 323–328 (2016).
24. Kunisaki, Y. et al. Arteriolar niches maintain haematopoietic stem cell quiescence. *Nature* **502**, 637–643 (2013).
25. Begum, S. et al. Characterization and engraftment of long-term serum-free human fetal liver cell cultures. *Cytotherapy* **12**, 201–211 (2010).
26. Zhang, K. et al. In vitro expansion of primary human hepatocytes with efficient liver repopulation capacity. *Cell Stem Cell* **23**, 806–819.e4 (2018).
27. Pal, D. et al. Fetuin-A acts as an endogenous ligand of TLR4 to promote lipid-induced insulin resistance. *Nat. Med.* **18**, 1279–1285 (2012).
28. Fitzgerald, K. A. & Kagan, J. C. Toll-like receptors and the control of immunity. *Cell* **180**, 1044–1066 (2020).
29. Chang, E. Y. et al. RECQ-like helicases Sgs1 and BLM regulate R-loop-associated genome instability. *J. Cell Biol.* **216**, 3991–4005 (2017).
30. Liang, Z. et al. Binding of FANCI–FANCD2 complex to RNA and R-loops stimulates robust FANCD2 monoubiquitination. *Cell Rep.* **26**, 564–572.e5 (2019).
31. Bayona-Feliu, A., Barroso, S., Munoz, S. & Aguilera, A. The SWI/SNF chromatin remodeling complex helps resolve R-loop-mediated transcription-replication conflicts. *Nat. Genet.* **53**, 1050–1063 (2021).
32. Wang, K. et al. Genomic profiling of native R loops with a DNA–RNA hybrid recognition sensor. *Sci. Adv.* **7**, eabe3516 (2021).
33. Crossley, M. P. et al. Catalytically inactive, purified RNase H1: a specific and sensitive probe for RNA–DNA hybrid imaging. *J. Cell Biol.* **220**, e202101092 (2021).
34. Enver, T. et al. Developmental impact of leukemic fusion genes on stem cell fate. *Ann. N. Y. Acad. Sci.* **1044**, 16–23 (2005).
35. Chen, L. et al. R-ChIP using inactive RNase H reveals dynamic coupling of R-loops with transcriptional pausing at gene promoters. *Mol. Cell* **68**, 745–757 (2017).
36. Niehrs, C. & Luke, B. Regulatory R-loops as facilitators of gene expression and genome stability. *Nat. Rev. Mol. Cell Biol.* **21**, 167–178 (2020).
37. Hong, D. et al. Initiating and cancer-propagating cells in TEL-AML1-associated childhood leukemia. *Science* **319**, 336–339 (2008).
38. Li, Z. et al. Leukaemic alterations of IKZF1 prime stemness and malignancy programs in human lymphocytes. *Cell Death Dis.* **9**, 526 (2018).
39. Brady, S. W. et al. The genomic landscape of pediatric acute lymphoblastic leukemia. *Nat. Genet.* **54**, 1376–1389 (2022).
40. Papaemmanuil, E. et al. Genomic classification and prognosis in acute myeloid leukemia. *N. Engl. J. Med.* **374**, 2209–2221 (2016).
41. Boiers, C. et al. A human IPS model implicates embryonic B-myeloid fate restriction as developmental susceptibility to B acute lymphoblastic leukemia-associated ETV6–RUNX1. *Dev. Cell* **44**, 362–377 (2018).

Publisher's note Springer Nature remains neutral with regard to jurisdictional claims in published maps and institutional affiliations.

Open Access This article is licensed under a Creative Commons Attribution-NonCommercial-NoDerivatives 4.0 International License, which permits any non-commercial use, sharing, distribution and reproduction in any medium or format, as long as you give appropriate credit to the original author(s) and the source, provide a link to the Creative Commons licence, and indicate if you modified the licensed material. You do not have permission under this licence to share adapted material derived from this article or parts of it. The images or other third party material in this article are included in the article's Creative Commons licence, unless indicated otherwise in a credit line to the material. If material is not included in the article's Creative Commons licence and your intended use is not permitted by statutory regulation or exceeds the permitted use, you will need to obtain permission directly from the copyright holder. To view a copy of this licence, visit http://creativecommons.org/licenses/by-nc-nd/4.0/.

© The Author(s) 2024

Methods

Human tissue acquisition

Human fetal liver tissues and cord blood samples were obtained from Tongji Hospital, Tongji University School of Medicine, Shanghai, China, with written informed consent from the parents and approval from the Medical Ethics Committee (k-w-2010-010) of Tongji Hospital. Fetal developmental age was estimated from measurements of crown–rump length and compared with a standard growth chart[42]. Plasma from infant patients with leukaemia and benign patients was obtained from Shanghai Children's Medical Center, Shanghai Jiao Tong University School of Medicine, Shanghai, China, with written informed consent from guardians of the patients and approval from the Medical Ethics Committee (SCMCIRB-K2024163-1) of the Shanghai Children's Medical Center.

Mice

B6.129P2-Gt(ROSA)26Sortm1(DTA)Lky/J, B6.Cg-Tg(Alb-cre)21Mgn/J, B6.Cg-Gt(ROSA)26Sortm14(CAG-tdTomato)Hze/J, C57BL/6J (B6-Ly5.2) and C57BL/6JGpt-*Fetua*-knockout (cas9) mice were maintained and bred in a pathogen-free facility in ventilated cages, a maximum of six mice per cage, on a 12-h day–night cycle, at 20–26 °C and 30–70% humidity, in compliance with the US National Institutes of Health Guide for the Care and Use of Laboratory Animals. For embryo collection, 8–10-week-old male and female mice were mated at night and then separated the next morning; the time of separation was considered E0.5. For colony-forming cell assays, whole-genome sequencing and leukaemic models, 3-week-old mice were used. Male and female mice were used in all experiments. Mice were placed into groups depending on their gestational days and genotypes; when possible, mice were randomized and the group allocation was blinded. No sample size calculation was performed. All animal experiments were approved by the Institutional Animal Care and Use Committees of Shanghai Jiao Tong University School of Medicine, Shanghai, China.

Isolation of human HSPCs

Liver tissues were processed immediately after isolation. The tissues were dissected into single-cell suspensions, and mononuclear cells were then separated using Ficoll density gradient centrifugation. Lineage-positive cells were depleted using the MagniSort Human Haematopoietic Lineage Depletion Kit (8804-6836-74, Thermo Fisher). Lineage-negative (Lin^-) cells were incubated with a combination of biotin-labelled lineage antibodies (to CD2, CD3, CD10, CD11b, CD14, CD16, CD19, CD56, CD123 and CD235a; 8804-6836-74, Invitrogen) and FITC-labelled CD34 (581; 555821, BD). After 15 min at 4 °C, the cells were washed with PBS, suspended in magnetic bead selection buffer (MACS; PBS, 2 mM EDTA and 0.5% BSA), and then incubated with streptavidin–phycoerythrin (12-4317-87, Thermo Fisher). After 10 min at room temperature, the cells were washed and suspended in IMDM (12440053, Thermo Fisher) supplemented with 1% BSA. Lin^- and $CD34^+$ HSPCs were subjected to flow cytometry on an Aria III flow cytometer (BD), and the data were collected using BD FACSDiva (V8.0.3). The HSPCs were cultured in StemSpan medium (09650, Stem Cell) supplemented with 10 ng ml^{-1} IL-6 (200-06, PeproTech), 10 ng ml^{-1} IL-3 (200-03, PeproTech), 10 ng ml^{-1} stem cell factor (SCF; 300-07, PeproTech) and 10 ng ml^{-1} Flt3 (300-19, PeproTech) at a concentration of 1×10^5 per millilitre for further experiments.

Isolation of mouse HSPCs

Pregnant mice were anaesthetized and euthanized by cervical dislocation. Placentas, fetal livers or bone tissues were then dissected into single-cell suspensions. Subsequently, the cells were incubated with biotin-labelled monoclonal antibodies targeting haematopoietic lineage markers (including B220, CD3, Gr-1 and Ter119; 88-7774-75, Thermo Fisher). After incubation, the cells were washed with MACS buffer and stained with streptavidin-conjugated magnetic beads (558451, BD). Following a 20-min incubation at 4 °C, the cells were washed again and resuspended in MACS buffer. Lineage-positive cells were depleted using a magnetic system. The Lin^- cells were then incubated with biotin-labelled lineage markers (88-7774-75, Thermo Fisher), phycoerythrin–Cy7-labelled Sca-1 (D7; 25-5981-82, Thermo Fisher), APC-labelled Kit antibodies (2B8; 17-1171-82, Thermo Fisher), phycoerythrin-labelled CD150 (mShad150; 12-1502-82, Thermo Fisher) and FITC-labelled CD48 antibodies (HM48-1; 11-0481-82, Thermo Fisher). After a 15-min incubation at 4 °C, the cells were washed with PBS and resuspended in MACS buffer. Streptavidin–phycoerythrin (12-4317-87, Thermo Fisher) or streptavidin–APC–Cy7 (405208, BioLegend) was added to the cells, which were then incubated for 10 min at room temperature. The cells were then washed and resuspended in IMDM supplemented with 1% BSA. LSK cells, lineage-negative, Sca-l-positive, Kit-positive, CD150-positive and CD48-negative cells (LT-HSCs), lineage-negative, Sca-l-positive, Kit-positive, CD150-negative and CD48-negative cells (ST-HSCs), and lineage-negative, Sca-l-positive, Kit-positive, CD150-negative and CD48-positive cells (MPPs) were flow-sorted according the gating strategy in Supplementary Fig. 1 in the Aria III flow cytometer (BD), and the data were collected using BD FACSDiva (v8.0.3). The HSPCs were cultured in StemSpan medium (09650, Stem Cell) supplemented with 10 ng ml^{-1} IL-6 (216-16, PeproTech), 10 ng ml^{-1} IL-3 (213-13, PeproTech) and 10 ng ml^{-1} SCF (250-03, PeproTech) at a concentration of 1×10^5 per millilitre for further experiments.

Isolation and culture of mouse fetal hepatocytes

To obtain Alb-Cre;ROSA26-LSL-tdTomato fetuses, we cross-mated B6.Cg-Tg(Alb-cre)21Mgn/J and B6.Cg-Gt(ROSA)26Sortm14(CAG-tdTomato)Hze/J mice. Fetal livers were then removed at E12.5 or E16.5 and digested with 0.6 mg ml^{-1} collagenase IV (17104019, Thermo Fisher) in Hank's balanced salt solution for 20 min at 37 °C. The digestion reaction was halted using cold PBS, and the mixture was subsequently centrifuged at 500 rpm for 5 min. Magnetic cell sorting (558451, BD) was used to remove blood cells expressing Ter119, B220, CD3, Gr-1 and Mac-1. Tomato-positive hepatocytes were flow-sorted using an MoFlo Astrios flow cytometer, and the data were collected using Summit (v6.3.1.16945; Beckman Coulter). The isolated hepatocytes were precultured in StemSpan medium (09650, Stem Cell) supplemented with hepatocyte growth supplement (1:100; 5201, ScienCell), 2 ng ml^{-1} IL-6 and 5% FBS (F2442, Sigma; referred to as SHIF) for 4 h. After removing the medium and non-adherent cells, the adherent hepatocytes were cultured in the same medium without FBS (referred to as SHI) for 20 h. The supernatant from the cultured fetal hepatocytes (referred to as conditioned SHI or co-SHI) was collected for further experiments.

Comet assay

The HSPCs at different development stages and HSPCs cultured with or without FetuA (100 μg ml^{-1}; 10318-H08H, SinoBiological) or ML216 (25 mM; S0469, Selleck) were treated with 20 μM etoposide (341205, Merck Millipore) for 30 min and then collected for the comet assay. A CometAssay kit from TREVIGEN (4250-050-k, R&D) was utilized to assess DNA damage. The alkaline method was utilized using the following steps: (1) 5,000 cells were mixed with 50 μl of melted LMAgarose (4250-050-02, R&D) at 37 °C and then pipetted onto a CometSlide; (2) the cells were then gelled for 3–5 min at 4 °C in the dark, followed by lysis with 4 °C lysis solution for 1 h; (3) the CometSlide was immersed in an alkaline unwinding solution (200 mM NaOH and 1 mM EDTA, pH > 13) for 1 h at 4 °C in the dark, and electrophoresis was conducted in the same solution at 20 V and 300 mA for 30 min at 4 °C); (4) the slides were washed twice with ddH_2O for 5 min each, followed by washing with 70% ethanol for 5 min, and the slides were then dried at room temperature overnight; and (5) the dried agarose was stained with SYBR Green I (A25742, Thermo Fisher) nucleic acid gel stain for 30 min. Images were

acquired with Las X (v4.7) on a Leica TCS Stellaris8 STED Microscope at ×20 resolution and analysed using OpenComet software (v1.3.1).

Immunofluorescence staining of cells

Human HSPCs treated with 80 μM etoposide (341205, Merck Millipore) for 30 min; mouse HSPCs treated with 20 μM etoposide for 30 min, 500 J m^{-2} ultraviolet radiation B (UVB) irradiation; human HSPCs cultured with or without FetuA (100 μg ml^{-1}; 10318-H08H, SinoBiological) for 2 h and then treated with 80 μM etoposide; mouse HSPCs cultured with co-SHI or hepatocytes for 2 h and then treated with 20 μM etoposide; and mouse HSPCs pre-treated with or without TLR4 antibody (1:50; 53-9041-80, Thermo Fisher) at 4 °C for 30 min and then cultured with or without FetuA (100 μg ml^{-1}; 50093-M08H, SinoBiological) for 2 h and thereafter treated with 20 μM etoposide were collected. These cells were then spun onto slides and fixed in 4% PFA for 10 min. After treatment with PBS containing 2% serum, 1% BSA and 0.2% Triton X-100, the cells were directly stained with primary antibodies overnight at 4 °C. Subsequently, the sections were stained with secondary antibodies for 1 h at room temperature. Phosphor-histone H2AX (Ser13; 20E3) rabbit monoclonal antibody (1:400; 9718S) was acquired from Cell Signaling Technology (CST), and TLR4 antibody (1:200; ab13556), mouse FetuA antibody (EPR17839-163; 1:100; ab187051) and p-RPA (phospho S33; 1:200; ab211877) were obtained from Abcam. Human FetuA antibody (1F6B9; 1:100; 66094-1-Ig) was obtained from Proteintech. The MYD88 (E11; 1:400; sc-74532) antibody was acquired from Santa Cruz. Images were acquired with ZEN (v2.3) on a Zeiss 880 Microscope at ×20 resolution or ×63 resolution, and analysed using ImageJ (v1.52p) and HALO (v3.6.4134).

Immunofluorescence staining of whole-mount tissues

Fetal livers and placentas were fixed in 4% PFA for 30 min, washed with PBS for 2–3 h, and stained with primary antibodies (diluted in PBS containing 1% BSA, 2% FCS and 0.5% Triton X-100) for 1–3 days. The tissues were then incubated with secondary antibodies for 2 h. Anti-mouse CD117 (Kit, ACK2; 1:50; 14-1172-85) was acquired from Thermo Fisher, and phospho-histone H2AX (Ser139; 20E3; 1:400; 9718S) rabbit monoclonal antibody was obtained from CST. Images were acquired with Las X (v4.7) on a Leica TCS Stellaris8 STED Microscope at ×20 resolution, and analysed using Image J (v1.52p) and Imaris (v9.0.1).

Immunofluorescence staining of tissue sections

Human or mouse placenta, fetal liver and bone tissues were fixed in 4% PFA for 30–60 min at room temperature (placenta and fetal liver tissues) or 5 h at 4 °C (bone tissues), dehydrated in 15% and 30% sucrose, and embedded in optimal cutting temperature compound at −20 °C. The tissues were then sectioned (20–25 μm) using a cryostat. The tissue sections were stained with primary antibodies for 6–12 h at 4 °C in PBS containing 1% BSA, 2% FCS and 0.5% Triton X-100. The sections were incubated with secondary antibodies for 1 h at room temperature. CD48–FITC (HM48-1; 1:100, 11-0481-82) was acquired from Thermo Fisher. APC-anti-lineage (Ter119 (1:400, 116212), Gr-1 (1:400, 108412), Mac-1 (1:400, 101212), B220 (1:400, 103212), CD3 (1:100, 100236), CD150-BV421 (SLAM; 1:100, 115925) and CD41-APC (MWReg30; 1:400, 133913)) were acquired from BioLegend. Kit goat monoclonal antibody (Gln25–Thr519; Ala207Glu; 1;400, AF1356) and anti-human serum albumin antibody (MAB1455; 1:200, 188835) were acquired from R&D. E-cadherin rabbit monoclonal antibody (24E10; 1:200, 3195T) and phospho-histone H2AX (Ser139; 20E3; 1:400, 9718S) rabbit monoclonal antibodies were acquired from CST. Laminin monoclonal antibody (1:200, ab11575), mouse FetuA antibody (EPR17839-163; 1:400, ab187051) and CD34 antibody (EP373Y; 1:100, ab81289) were acquired from Abcam. CD45–FITC (104; 1:100, MCD45201) was acquired from Invitrogen. Nestin antibody (1:50, AN205-1) was acquired from Beyotime. E-cadherin antibody (DECAM-1; 1:200, sc-59778) was acquired from Santa Cruz. CD144 antibody (1:200, 550548) and Sca-1 antibody (D7; 1:200, 557403) were acquired from BD. Human FetuA antibody (1F6B9; 1:200, 66094-1-Ig) was acquired from Proteintech. Images were acquired with ZEN (v2.3) on a Zeiss 880 Microscope at ×20 resolution or ×63 resolution, and analysed using ImageJ (v1.52p), Imaris (v9.0.1) and HALO (v3.6.4134).

Colony-forming cell assay

The assay was performed in a semi-solid methycellulose medium (03434, Stem Cell Technologies) following the technical manual. In brief, the sorted HSPCs were plated in methycellulose in a 35-mm dish (200 cells per dish). Cultures were incubated at 37 °C in a humidified incubator (more than 95%) with 5% CO_2 in the air. The colonies were scored under a microscope 10–12 days post-plating. Replating was performed by pooling total cells from primary cultures and inoculating 10^4 cells into fresh methycellulose medium.

Metaphase chromosome preparation and FISH

Bone marrow Lin^- cells were incubated with 0.05 μg ml^{-1} colcemid for 1 h at 37 °C and then centrifuged at 400*g* for 10 min. The cells were suspended in 1 ml of hypotonic solution (0.075 M KCl) for 30 min at 37 °C, and the reaction was stopped by the addition of freshly prepared fixative solution (3:1 methanol:glacial acetic acid). The cells were then subjected to three rounds of fixative changes. After that, the cells were dropped onto slides and allowed to dry at room temperature. Two-colour FISH was performed using whole-chromosome probes for mouse chromosome 4 (FITC; D-1404-050-FI, MetaSysterms) and chromosome 6 (Texas red; D-1406-050-OR, MetaSysterms), and counterstaining was performed with DAPI-Antifade solution. Images were acquired with Las X (v4.7) on a Leica TCS Stellaris8 STED Microscope at ×20 resolution and analysed using Image J (v1.52p).

Mouse models of leukaemia

Three-week-old mice were intraperitoneally injected with 80 mg kg^{-1} *N*-ethyl-*N*-nitrosourea (ENU; N3385, Sigma) four times, which was administered twice a week, and the mice were monitored by daily observation of leukaemic symptoms and signs including fired hair, white toes, swollen lymph nodes and loss of body weight, and weekly measurement of leukaemia-like cells by Gimsa staining of peripheral blood smears. Once these appeared, the animals were killed, and the disease of leukaemia was determined by exhibition of enlarged spleens and lymph nodes, increased proportions of immature Lin^- cells in the bone marrow and leukaemic cell infiltration in spleens and bone marrow shown by haematoxylin and eosin staining of the tissue sections.

Western blot

After treatment with or without FetuA (100 μg ml^{-1}; 50093-M08H, SinoBiological) for 2 h, mouse HSPCs (LSK) were lysed and blotted with bZIP antibody and their phosphorylated forms. After treatment with or without FetuA (100 μg ml^{-1}; 50093-M08H, SinoBiological) and the bZIP inhibitor SR11032 (2 mM; HY-15870, MedChemExpress) for 6 h, mouse Lin^- haematopoietic cells were lysed and blotted with BLM antibody. The cells were lysed using SDS lysis buffer. The lysates were then separated on SDS-polyacrylamide gels and transferred to nitrocellulose membranes (Bio-Rad). Western blotting was carried out using the following primary antibodies: FetuA (1:2,000), JunB (1:1,000), phosphorylated JunB (p-JunB; 1:1,000), Jun (1:1,000), p-Jun (1:1,000), Fosl1 (1:10,000), p-Fosl1 (1:1,000), BLM (1:500) and laminB1 (1:2,000). The membranes were incubated overnight at 4 °C with primary antibodies. After rinsing to remove any unbound primary antibody, the membranes were exposed to a horseradish peroxidase-conjugated secondary antibody at room temperature for 1 h. The secondary antibody was detected using chemiluminescence (WBKLS0500, Merck Millipore). The following primary antibodies were used: anti-p-JunB (Thr102/Thr104; 8053S) and anti-p-Fosl1 (S265; 3880S) from CST and anti-JunB (EPR6518; ab128878), anti-Fosl1 (ab232745), anti-p-Jun

(phospho S63; ab32385), anti-Jun (EP693Y; ab40766), anti-laminB1 (EPR8985; ab133741) and anti-FetuA (EPR17839-163; ab187051) from Abcam, and anti-BLM (B-4; sc-365753) from Santa Cruz. The intensity of bands was measured using ImageJ (v1.52p). For gel source data, see Supplementary Fig. 2.

Mass spectrometry analysis

SHI and co-SHI media, E12.5 and E16.5 fetal liver tissues and bone marrow plasma samples from infants were collected for data-independent acquisition tandem mass spectrometry (DIA MS/MS) analysis. The medium samples were treated with 2% SDS buffer containing 50 mM dithiothreitol for 20 min at room temperature and then boiled at 100 °C for 5 min. The protein samples were alkylated in the dark at room temperature for 1 h by adding 200 mM iodoacetamide. To precipitate the proteins, a 5× volume of pre-cooled acetone was used overnight at −20 °C. The tissue samples were diluted with 50 mM NH_4HCO_3 and centrifuged three times at 20 °C and 14,000*g* using YM-10 filter units. The protein lysates were reduced for 1 h at room temperature with a final concentration of 10 mM dithiothreitol and then alkylated for 1 h in the dark at room temperature with a final concentration of 55 mM iodoacetamide. The protein mixtures were exchanged with 50 mM NH_4HCO_3 by centrifugation at 20 °C and 14,000*g* three times. The protein precipitates were digested overnight at 37 °C at a protein-to-enzyme ratio of 50:1 with trypsin. Tryptic peptides were collected by centrifugation at 20 °C and 14,000*g* for 20 min. The peptides were then treated with 1% trifluoroacetic acid, purified using C18 Ziptips and eluted with 0.1% trifluoroacetic acid in 50–70% acetonitrile. The eluted peptides were dried using a SpeedVac (Thermo Savant) and resuspended in 1% formic acid and 5% acetonitrile. Before analysis, indexed retention time (iRT) peptides (Biognosys) were spiked into the samples following the manufacturer's instructions. The pooled digestates were dried using a SpeedVac (Thermo Savant) and resuspended in 5% ACN in 0.05 M ammonium formate. The digested peptides were fractionated using high-pH reversed-phase separation on a Dionex ultra-high-performance liquid chromatography (Thermo Scientific) with a 2.1 × 150 mm ethylene-bridged hybrid (BEH) C18 3-µm column at 40 °C, with a flow rate of 0.2 ml min^{-1} and a 60-min ACN gradient (5–30%) in 5 mM ammonium formate (pH 10). Fractions were collected at 1-min intervals and pooled at various intervals, resulting in up to 12 fractions. The samples were dried and resuspended in 1% formic acid and 5% acetonitrile. Data-dependent acquisition (DDA) analysis was conducted on an Orbitrap Fusion LUMOS mass spectrometer (Thermo Fisher Scientific) connected to an Easy-nLC 1200 via an Easy Spray (Thermo Fisher Scientific). The peptide mixtures were loaded onto a self-packed analytical PicoFrit column (75 µm × 40 cm) with an integrated spray tip (New Objective) packed with ReproSil-Pur 120A C18-AQ 1.9 µm (Dr. Maisch GmbH). The peptides were separated using a 120-min linear gradient from 95% solvent A (0.1% formic acid, 2% acetonitrile and 98% water) to 28% solvent B (0.1% formic acid and 80% acetonitrile) at a flow rate of 250 nl min^{-1} at 50 °C. The mass spectrometer was operated in positive-ion mode and used the data-dependent mode with a specialized cycle time (3S) to automatically switch between MS and MS/MS scans. A full MS scan from 350 to 1,500 m/z was acquired at a resolution of R = 120,000 (defined at m/z = 400). MS/MS scans were performed at a resolution of 30,000, with an isolation window of 4 Da and higher-energy collisional dissociation fragmentation with a collision energy of 30 ± 5%. Dynamic exclusion was set to 30 s. Sequences were identified using the mouse UniProt fasta database (53,099 entries, downloaded on 4 November 2018) with default parameters. The digestion enzyme used was a specific trypsin enzyme with two missed specialized cleavages. Carbamidomethyl of cysteine was set as a fixed modification, and oxidation of methionine was set as a variable modification. The iRTs derived from median iRTs across all DDA runs were calculated. Fragment ions for the targeted data analysis were selected from 300 to 1,800 m/z, with a minimal relative intensity set to more than 5% and a fragment ion number greater than 3. The false discovery rate (FDR) was set to 1% for protein and peptide spectrum matches. Protein inference was performed using the ID Picker algorithm integrated within the Spectronaut software. DIA MS/MS acquisition was performed using the same liquid chromatography-MS systems and liquid chromatography linear gradient method as DDA. For MS/MS acquisition, the DIA method was set with 50 variable isolation windows based on the full-width at half-maximum and constructed using the respective DDA data. The full scan was set at a resolution of 1,200,000 over a m/z range of 350–1,500, followed by DIA scans at a resolution of 30,000. The collision energy (CE), auto gate control (AGC) and maximal injection time were set to 30 ± 5%, 1×10^6 and 54 ms, respectively. The DIA raw files were analysed using Spectronaut X (Biognosys). The retention time prediction type was set to dynamic iRT, and a correction factor was applied for window 1. Interference correction at the MS2 level was enabled. Systematic variance was normalized using a local normalization strategy. The FDR was estimated using the mProphet approach and set to 1% at the peptide precursor and protein levels. Protein intensity was calculated by summing the intensities of their respective peptides, which were measured using the peak areas of their fragment ions in MS2 and multiplied by a factor based on the total sample volume of each sample. All the results were filtered with a Q value cut-off of 0.01 (corresponding to a 1% FDR).

Intraplacental injection of FetuA

The pregnant mice were anaesthetized using 3.5% chloral hydrate and then secured onto a heating pad with all four legs immobilized. The abdominal surface was shaved and disinfected with 75% alcohol. A longitudinal incision measuring 1–1.5 cm in length was made on the abdominal skin, and the peritoneum was cut. Cotton gauze was placed around the incision. One uterine horn was carefully exposed and pulled out using blunt forceps onto gauze soaked in PBS. The uterus was held in place with blunt forceps, and recombinant FetuA (10 µg per 15 µl each) was injected into the placenta. After the injection, the uterus was carefully returned to the abdomen, ensuring that it was positioned exactly as before. The peritoneum was closed with a haemostat. Two hours later, 5 mg kg^{-1} etoposide was administered through intraperitoneal injection. The fetuses were harvested after 1 h and fixed for immunofluorescence assays.

ATAC-seq library preparation and sequencing

ATAC-seq libraries were prepared as previously described[43]. In brief, HSPCs were lysed using lysis buffer containing 10 mM Tris-HCl (pH 7.4), 10 mM NaCl, 3 mM $MgCl_2$ and 0.1% IGEPAL CA-630 for 10 min before being spun at 4 °C to obtain nuclear preparations. The supernatant was discarded, and the nuclei were then incubated with Tn5 transposome and tagmentation buffer at 37 °C for 30 min (Vazyme). The resulting tagmentation products were purified and amplified using PCR. PCR amplification involved ten cycles under the following conditions: 72 °C for 5 min; 98 °C for 30 s; thermocycling at 98 °C for 10 s, 63 °C for 30 s and 72 °C for 1 min; and 72 °C for 5 min. The libraries were purified using a PCR purification kit (28004, Qiagen), and the fragments were enriched using 0.5× and 1.0× VAHTS DNA Clean Beads (N412-01, Vazyme) after amplification.

ATAC-seq data processing

All reads were aligned to the mm10 genome using the Burrows-Wheeler Aligner (BWA-MEM) after trimming the adapter sequences with Trim_Galore (v0.6.7). Low-quality reads were filtered out, whereas PCR duplicates and reads mapped to the mitochondria or the Y chromosome were discarded. The remaining reads on the left were shifted (+4/−5) to correct Tn5 enzyme insertions based on the read strands. Peak calling was performed using MACS2 (v2.2.6) with the following options: -f BAM, -g mm, --nomodel, --shift -100 and --extsize 200. The samples were normalized using the bamCoverage function from deepTools (v3.5.1) to visualize the signal in IGV (v2.7.0).

Quality control of ATAC-seq data was conducted, and correlation analysis was performed using deepTools (v3.5.1). The fragment distribution was generated using ATAC-seq QC (v1.14.4). The peak atlas was obtained by expanding the peak summit by ±500 bp, and differential peaks were identified using DESeq2 (v1.26.0). DNA-binding factor motifs were analysed by determining the motifs in the differential peaks using HOMER (v4.11). ATAC signals were visualized as a heatmap using the complexHeatmap package (v2.2.0).

RNA-seq and analysis

Total RNA was extracted from cultured or non-cultured HSPCs using Tri Pure Isolation Reagent (11667157001) from Roche following the manufacturer's instructions. The quality of the RNA was assessed using the Fragment Analyser platform. High-quality samples were chosen for library construction using the Illumina TruSeq RNA Prep Kit (20015949). The libraries were subsequently sequenced on the Illumina HiSeq4000 platform, generating 2 × 150 bp paired-end reads. To process the raw data, Trim Galore (v0.6.7) was used with the following parameters: '--quality 20 --fastqc --length 20 --stringency 1'. The resulting clean reads were then aligned to the mouse reference genome (mm10) using hisat2 (v2.2.1). GENCODE annotations (gencode.vM25.annotation.gtf; downloaded in April 2021) and HTSeq-count (v0.13.5) were used to assign the aligned reads to genes. Subsequently, the counts were normalized to fragments per kilobase of transcript per million mapped reads (FPKM), and log(FPKM + 1) was utilized to analyse the overall similarity or dissimilarity between the samples.

Cut&Tag library preparation and sequencing

The Hyperactive Universal Cut&Tag Assay Kit for Illumina Pro (TD904, Vazyme) was used in this study. In summary, 1×10^5 LSK cells treated with or without FetuA were collected and washed in 500 µl of wash buffer. The cells were then resuspended in 100 µl of wash buffer. Subsequently, 10 µl of concanavalin A-coated magnetic beads were activated and added to 1×10^5 cells. The cells were incubated at room temperature for 10 min, after which the supernatant was removed. The resulting bead-bound cells were resuspended in 50 µl of antibody buffer. Next, 1 µl of Jun rabbit monoclonal antibody (60A8; 9165T, CST), JunB rabbit monoclonal antibody (C37F9; 3753S, CST) or Fosl1 mouse monoclonal antibody (C-12; sc-28310, Santa Cruz) was added and incubated with the bead-bound cells overnight at 4 °C with rotation. The supernatant was then removed, and the bead-bound cells were resuspended in 50 µl of dig-wash buffer containing goat anti-rabbit IgG antibody (Ab207-01-AA, Vazyme) or goat anti-mouse IgG antibody (Ab208-01-AA, Vazyme; diluted 1:100). This mixture was incubated at room temperature for 1 h. The bead-bound cells were washed three times with 200 µl of dig-wash buffer to remove any unbound antibodies. Next, 2 µl of the pA-Tn5 adapter complex was diluted in 98 µl of dig-300 buffer and mixed with the bead-bound cells. The mixture was subjected to rotation at room temperature for 1 h. The bead-bound cells were washed three times with 200 µl of dig-300 buffer to eliminate any unbound pA-Tn5 protein. The cells were then resuspended in 50 µl of tagmentation buffer and incubated at 37 °C for 1 h. To terminate the tagmentation reaction, 2 µl of SDS was added to the cells and incubated for an additional 10 min at 55 °C. The tagmentation products were purified using DNA Extract Beads Pro and eluted in 15 µl of nuclease-free water. For generation of the sequencing libraries, the DNA tagments were mixed with a universal i5 primer and a unique i7 primer and amplified using 2× Cut &Tag amplification mix. The resulting PCR products were purified using VAHTS DNA lean beads (N411, Vazym), and subsequently analysed using an Agilent 2100 Bioanalyzer and Illumina Novaseq 6000.

Cut&Tag data processing

Cut&Tag reads were aligned to the mm10 genome with Bowtie2 (v2.3.5.1) using the following parameters: --end-to-end --very-sensitive --no-mixed --no-discordant --phred33 -I10 -X700. Duplicate reads were removed with Picard (v2.25.5). The track files were made with the bamCoverage command from deepTools (v3.5.1). Cut&Tag peaks were called using MACS2 (v2.2.6). The distribution of Cut&Tag peaks was annotated with the R package ChIPseeker (v1.22.1).

R-loop staining

HSPCs from E12.5 placenta, E12.5 fetal liver, E16.5 fetal liver or E12.5 FL-HSPCs with or without FetuA (100 µg ml^{-1}; 50093-M08H, SinoBiological) or ML216 (25 mM; S0469, Selleck) treatment for 2 h were collected. The cells were spun onto slides, fixed in 4% PFA for 10 min and washed three times with PBS. After permeabilization with PBS containing 0.3% Triton X-100 for 10 min at room temperature, the cells were washed three times with PBS and then blocked with PBS containing 2% serum, 1% BSA and 0.2% Triton X-100 for 1 h at 37 °C. Immunofluorescence experiments with the dRNH1 protein were performed as previously described[33]. In brief, the cells were incubated with 30 µl dRNH1 (0.24 mg ml^{-1}) for 1 h at 37 °C, followed by three washes with PBS. The cells were then incubated with 1 µg ml^{-1} DAPI for 10 min. For immunofluorescence experiments with the GST-His6-2×HBD protein[32], the cells were incubated with 30 µl GST-His6-2×HBD (2 µg ml^{-1}) overnight at 4 °C. After three washes with PBS, the cells were stained with an anti-HisTag monoclonal antibody (AMC0149; 1:400; AE003, ABclonal) for 1 h at room temperature, followed by three washes with PBS. The cells were then stained with a rabbit anti-mouse IgG antibody (1:400; SPA231, Solarbio) for 1 h at room temperature. After three washes with PBS, the cells were incubated with 1 µg ml^{-1} DAPI for 10 min. Images were acquired using a Zeiss 880 microscope, and the signal intensity was measured using HALO (v3.6.4134).

R-loop Cut&Tag library preparation and sequencing

The R-loop Cut&Tag library was prepared following protocols previously described[32] with minor modifications. For this experiment, the Hyperactive Universal Cut&Tag Assay Kit for Illumina (TD903, Vazyme) was utilized. In brief, 1×10^5 cells were gently pipetted and washed twice in 500 µl of wash buffer. Then, 10 µl of concanavalin A-coated magnetic beads was activated and added to the 1×10^5 cells, followed by incubation at room temperature for 10 min. The supernatant was then removed, and the bead-bound cells were resuspended in 90 µl of antibody buffer. Subsequently, 10 µl of recombinant GST-His6-2×HBD (0.2 mg ml^{-1}) protein was added and the mixture was incubated with the bead-bound cells overnight at 4 °C with rotation. After two washes with dig-wash buffer, the samples were incubated with an anti-HisTag monoclonal antibody (AMC0149; 1:400; AE003, ABclonal) for 1 h at room temperature, followed by incubation with a rabbit anti-mouse IgG antibody (final concentration, 10 µg ml^{-1}; SPA231, Solarbio) for 1 h at room temperature. Unbound antibodies were removed by three brief washes with 200 µl of dig-wash buffer. To facilitate tagmentation, 2 µl of a pA-Tn5 adapter complex was diluted in 98 µl of dig-300 buffer and mixed with bead-bound cells, which were then rotated at room temperature for 1 h. After three washes in 200 µl of dig-300 buffer to remove unbound pA-Tn5 protein, the cells were resuspended in 50 µl of tagmentation buffer and incubated at 37 °C for 1 h. The tagmentation reaction was stopped by adding 1.8 µl of 0.5 M ethylenediaminetetraacetic acid, 0.6 µl of 10% SDS, 5 µl of nuclease-free water and 1 µl of proteinase K (20 mg ml^{-1}), and further incubated at 55 °C for 60 min. Following purification with 1× DNA clean beads (Vazyme Biotech), the resulting tagmentation products were eluted in 10 µl of nuclease-free water. For the strand displacement reaction, the eluent was mixed with 10 U of Bst 2.0 WarmStart DNA polymerase (M0538, NEB) in 1× Q5 polymerase reaction buffer and incubated at 65 °C for 30 min. The reaction was then halted by incubation at 80 °C for 20 min. To generate the sequencing libraries, the mixture was combined with a universal i5 primer and a uniquely barcoded i7 primer and subsequently amplified using Q5 high-fidelity master mix (M0491, NEB). The libraries were size selected with 0.56–0.85× DNA clean beads and subjected to analysis using an Agilent 2100 Bioanalyzer and Illumina PE150 sequencing.

R-loop Cut&Tag data processing

The Cut&Tag data were processed as previously described[32]. In summary, Cut&Tag reads were aligned to the mm10 genome using Bowtie2 (v2.3.5.1), allowing for uniquely mapped reads with up to two mismatches. The aligned reads were normalized to the total number of reads (reads per million). Subsequently, track files were generated using the bamCoverage command from deepTools (v3.5.1). Cut&Tag peaks were called using MACS2 (v2.2.6), and the distribution of Cut&Tag peaks was annotated using the R package ChIPseeker (v1.22.1). The average coverage was used to create metaplots within the indicated windows. Gene Ontology enrichment analysis was performed using clusterProfiler (v3.14.3), and circus-plots were generated using circlise (v0.4.8).

Whole-genome sequencing of mouse HSPCs

Genomic DNA was extracted using the QIAamp DNA Mini Kit (51304, Qiagen) following the manufacturer's protocol. Whole-genome sequencing was conducted as previously described[44]. In brief, short-insert 350-bp genomic libraries were constructed following Illumina library protocols, and sequencing was performed on an Illumina NovaSeq 6000 platform using 150-base paired-end reads, achieving an average coverage of 30×. The sequence data were mapped to the mouse genome reference mm10 using the BWA-MEM algorithm. Unmapped reads and PCR-derived duplicates were excluded from the analysis. Insertions and deletions (indels) and structural variants were called using the Pindel and BreakDancer algorithms, respectively, as described elsewhere[45,46]. The group treated with saline was used as germline control.

Cell cycle analysis of mouse HSPCs by combining Hoechst and pyronin Y

The cells were harvested from E12.5 placenta, E12.5 fetal liver and E16.5 fetal liver samples, and lineage-positive cells were depleted using a magnetic system. The Lin^- cells or Lin^- cells cultured with or without FetuA (100 μg ml^{-1}; 50093-M08H, SinoBiological) or ML216 (25 mM; S0469, Selleck) for 2 h were collected. The cells were then suspended in 1 ml of StemSpan medium (09650, Stem Cell). Hochest33342 (10 μg ml^{-1}; b2261-25mg, Sigma) and verapamil (50 μM; M14204, AbMole) were added to the cell suspension. The mixture was thoroughly mixed and incubated at 37 °C for 60 min in the dark. Subsequently, 5 μl of 100 μg ml^{-1} pyronin Y (213519-1g, Sigma) was directly added to the cells, followed by continuous incubation at 37 °C for another 15 min in the dark. After centrifugation at 300*g* for 5 min at 4 °C, the cells were suspended in MACS buffer and incubated with biotin-labelled lineage markers (88-7774-75, Thermo Fisher), FITC-labelled Sca-1 (E13-161.7; 122506, BioLegend) and APC-labelled Kit antibodies (2B8; 17-1171-82, Thermo Fisher). Following a 15-min incubation at 4 °C, the cells were washed with PBS, suspended in MACS buffer and incubated with streptavidin–APC–Cy7 (405208, BioLegend). After another 15 min at 4 °C, the cells were washed and resuspended in MACS buffer. The samples were analysed using a Beckman cytoFLEX LX, and the data were analysed using FlowJo (v10).

DNA synthesis analysis of mouse HSPCs by EdU

Pregnant mice were administered intraperitoneal injections of 100 mg kg^{-1} EdU (CX000, CellularLab) 2 h before being killed. Cells were collected from E12.5 placenta, E12.5 fetal liver and E16.5 fetal liver and subjected to lineage-positive cell depletion using a magnetic system. The cells were then incubated with biotin-labelled lineage markers (88-7774-75, Thermo Fisher), phycoerythrin–Cy7-labelled Sca-1 (D7; 25-5981-82, Thermo Fisher) and APC-labelled Kit (2B8; 17-1171-82, Thermo Fisher) antibodies. After 15 min at 4 °C, the cells were washed with PBS, suspended in MACS buffer and incubated with streptavidin–phycoerythrin. EdU was detected using the EdU Cell Proliferation Kit with Alexa Fluor 488 (CX002, CellularLab) following the manufacturer's instructions. The samples were analysed on a Beckman cytoFLEX LX, and the data were analysed using FlowJo (v10).

Cell cycle analysis of mouse HSCs and MPPs by Ki67

Harvested cells from E12.5 placenta, E12.5 fetal liver and E16.5 fetal liver were subjected to lineage-positive cell depletion using a magnetic system. The cells were incubated with biotin-labelled lineage markers (88-7774-75, Thermo Fisher), phycoerythrin–Cy7-labelled Sca-1 (D7; 25-5981-82, Thermo Fisher), APC-labelled Kit (2B8; 17-1171-82, Thermo Fisher), phycoerythrin-labelled CD150 (mShad150; 12-1502-82, Thermo Fisher) and APC–Cy7-labelled CD48 (HM48-1; 103431, BioLegend) antibodies. Following a 15-min incubation at 4 °C, the cells were washed with PBS, suspended in MACS buffer and then incubated with streptavidin–Percpcy5.5. After another 15 min at 4 °C, the cells were fixed and permeabilized with Foxp3/Transcription Factor Staining Buffer Set Kit (00-5523-00, Invitrogen) according to the manufacturer's instructions. Subsequently, the samples were incubated with FITC-labelled Ki67 (SolA15; 11-5698-80, Thermo Fisher). After a 30-min incubation at 4 °C, the cells were washed with permeabilization buffer and analysed using a Beckman CytoFLEX LX, and the data were analysed using FlowJo (v10).

RNA synthesis analysis of mouse HSPCs by ethyluridine

Pregnant mice were injected intraperitoneally with 50 mg kg^{-1} ethyluridine (2469–25 mg, Lumiprobe) 1 h before being killed. Cells were collected from E12.5 placenta, E12.5 fetal liver and E16.5 fetal liver and subjected to lineage-positive cell depletion using a magnetic system. The cells were then incubated with biotin-labelled lineage markers (88-7774-75, Thermo Fisher), FITC-labelled Sca-1 (E13-161.7; 122506, BioLegend) and APC-labelled Kit (2B8; 17-1171-82, Thermo Fisher) antibodies. After 15 min at 4 °C, the cells were washed with PBS, suspended in MACS buffer and incubated with streptavidin–APC–Cy7 (405208, BioLegend). The ethyluridine was stained using the Cell-Light EU Apollo567 RNA Imaging Kit (C10316-1, RIBOBIO) according to the manufacturer's instructions. The samples were analysed on a Beckman cytoFLEX LX, and the data were analysed using FlowJo (v10).

Statistics

Statistics analyses were performed using R (v.3.6.3) and GraphPad Prism (v.9.5). *n* Denotes biological replicates. For violin plots in all panels, the median and quartiles are shown. For boxplots, the mean ± s.d. is shown. For boxplots in Fig. 5c and Extended Data Fig. 9e,i, the median and quartiles are shown. For boxplots in Fig. 5d and Extended Data Fig. 3b, the boxes delimit the minima and maxima, and the horizontal line represents the mean. For survival analysis, the long-rank test was used to compare the difference between groups. For correlation analysis, the Pearson test was used. For comparing two groups, the unpaired Student's *t*-tests and Wilcoxon tests were used. $P < 0.05$ was considered to be significant.

Reporting summary

Further information on research design is available in the Nature Portfolio Reporting Summary linked to this article.

Data availability

The ATAC-seq, RNA-seq, R-loop Cut&Tag sequencing, bZIP Cut&Tag sequencing and whole-genome sequencing data reported in this paper have been deposited in the Genome Sequence Archive in BIG Data Center, Beijing Institute of Genomics (BIG), Chinese Academy of Sciences, under the study accession number PRJCA026810. The reference genome used was mm10 (https://hgdownload.soe.ucsc.edu/goldenPath/mm10/bigZips/mm10.fa.gz). The annotation dataset used in the RNA-seq analysis was gencode.vM25.annotation.gtf (http://ftp.ebi.ac.uk/pub/databases/gencode/Gencode_mouse/release_M25/gencode.vM25.annotation.gtf.gz). Source data are provided with this paper.

Code availability

This paper did not generate new code and new software.

42. Corton, M. M., Leveno, K. J., Bloom, S. L. & Hoffman, B. L. *Williams Obstetrics* 24th edn (McGraw Hill, 2014).
43. Buenrostro, J. D., Wu, B., Chang, H. Y. & Greenleaf, W. J. ATAC-seq: a method for assaying chromatin accessibility genome-wide. *Curr. Protoc. Mol. Biol.* **109**, 21–29 (2015).
44. Behjati, S. et al. Genome sequencing of normal cells reveals developmental lineages and mutational processes. *Nature* **513**, 422–425 (2014).
45. Raine, K. M. et al. cgpPindel: identifying somatically acquired insertion and deletion events from paired end sequencing. *Curr. Protoc. Bioinformatics* **52**, 11–17 (2015).
46. Chen, K. et al. BreakDancer: an algorithm for high-resolution mapping of genomic structural variation. *Nat. Methods* **6**, 677–681 (2009).

Acknowledgements We thank G.-L. Xu for discussing the data and critical reading of the manuscript; L.-J. Hui for assisting with the culture of the fetal hepatocytes; and the Core Facility of Basic Medical Science in Shanghai Jiao Tong University School of Medicine for technical support. This work was supported by grants from the National Natural Science Foundation of China (81920108005, U23A20417, 81730007, 31872842, 91442106, 81120108006, 90919055 and 81721004) and from the CAMS Innovation Fund for Medical Sciences (CIFMS; 2019-I2M-5-051).

Author contributions X.-L.G. designed the experiments and composed the figures. Lei Chu and H.Z. supplied the human samples. X.-L.G., Y.-D.W., Y.-J.L., Y.H., R.-Y.W., H.-Y.X., F.K. and Z.-Y.X. performed the experiments. Y.-D.W., R.-Y.W. and J.Y. analysed the ATAC-seq data. Y.-D.W., S.-P.L. and R.-Y.L. analysed the RNA-seq data. Y.-D.W. analysed the R-loop Cut&Tag data. Y.-D.W. and Y.-J.L. analysed the whole-genome sequencing data. G.-H.L. and Lei Chen provided advice for the ATAC-seq analysis. Liang Chen provided advice for the R-loop Cut&Tag analysis. Lei Chen, G.-Q.C., Liang Chen, F.B., T.E., G.-H.L. and H.-F.L. discussed the data and the manuscript. D.-L.H. conceived and supervised the project, analysed the data and wrote the manuscript.

Competing interests The authors declare no competing interests.

Additional information

Supplementary information The online version contains supplementary material available at https://doi.org/10.1038/s41586-024-08307-x.

Correspondence and requests for materials should be addressed to Deng-Li Hong.

Peer review information *Nature* thanks John Chute, Stephan Hamperl and the other, anonymous, reviewer(s) for their contribution to the peer review of this work. Peer reviewer reports are available.

Reprints and permissions information is available at http://www.nature.com/reprints.

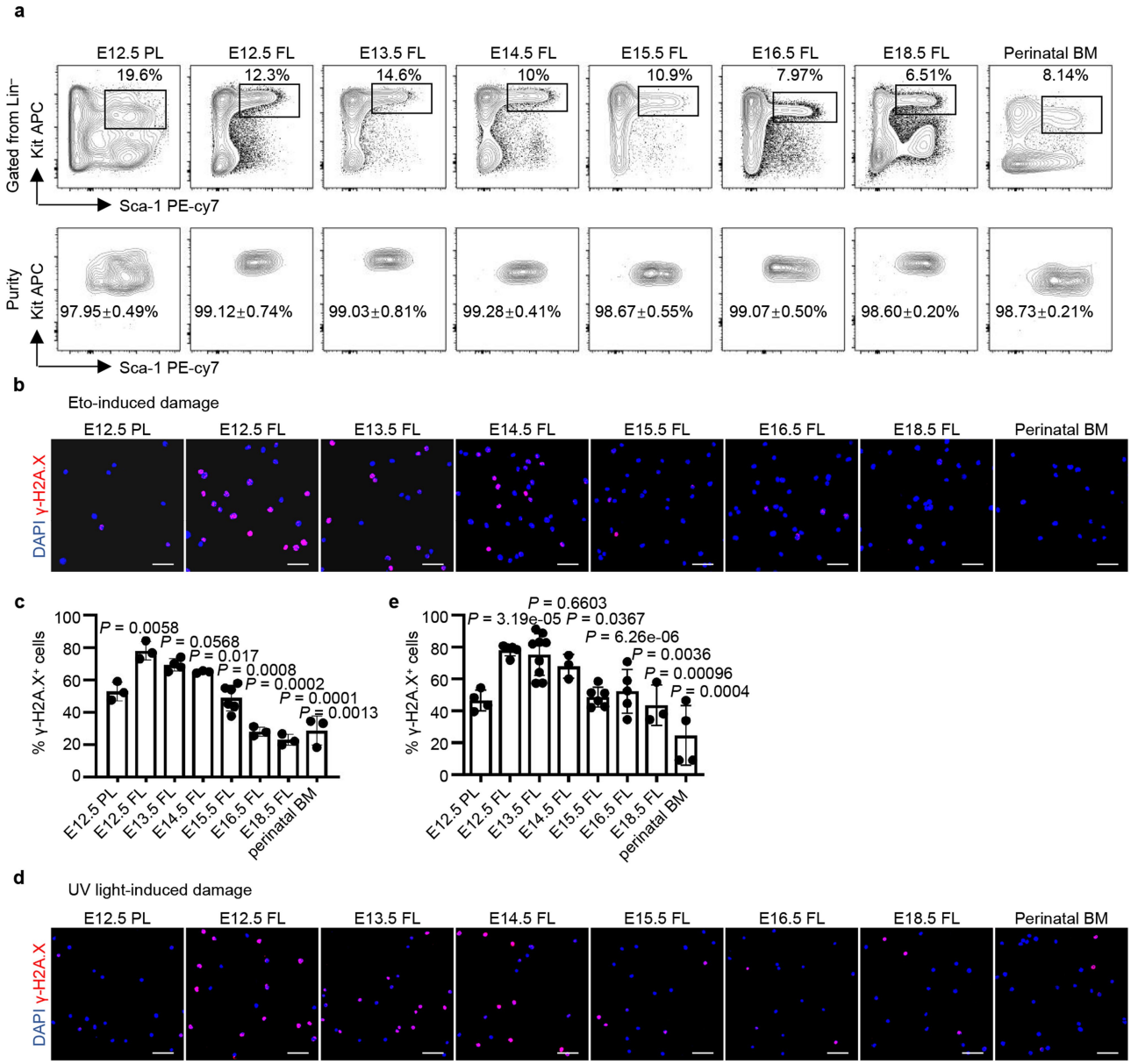

Extended Data Fig. 1 | Flow-sorting of HSPCs and their sensitivity to genotoxic agents ex vivo. a, Immunophenotypically negative lineage (Lin^-), positive Sca-l ($Sca\text{-}1^+$) and Kit^+ (LSK) cells were sorted by flow cytometry with high purities (mean ± s.d.) from the haematopoietic tissues of the E12.5 placenta (PL) ($n = 4$), E12.5 fetal liver (FL) ($n = 6$), E13.5 FL ($n = 4$), E14.5 FL ($n = 4$), E15.5 FL ($n = 3$), E16.5 FL ($n = 3$), E18.5 FL ($n = 5$) and perinatal bone marrow (BM) ($n = 3$) to assay the sensitivity of HSPCs to genotoxic agents. **b, c**, Representative fluorescence images and positive cell proportions of γ-H2AX etoposide (Eto)-induced ex vivo in HSPCs isolated from PL, FL and BM on different embryonic days (E13.5 FL, $n = 4$; E15.5 FL, $n = 6$; other groups, $n = 3$). Scale bar, 50 µm. **d, e**, Representative fluorescence images and positive cell proportions of γ-H2AX ultraviolet (UV) light-induced HSPCs isolated from PL, FL and BM on different embryonic days (E12.5 PL, Perinatal BM, $n = 4$; E12.5 FL, E16.5 FL, $n = 5$; E13.5 FL, $n = 9$; E14.5 FL, E18.5FL, $n = 3$; E15.5 FL, $n = 6$). Scale bar, 50 µm. The n represents independent experiments. The mean ± s.d. is shown (**c, e**). Statistical tests: unpaired two-sided Student's t-test (**c, e**).

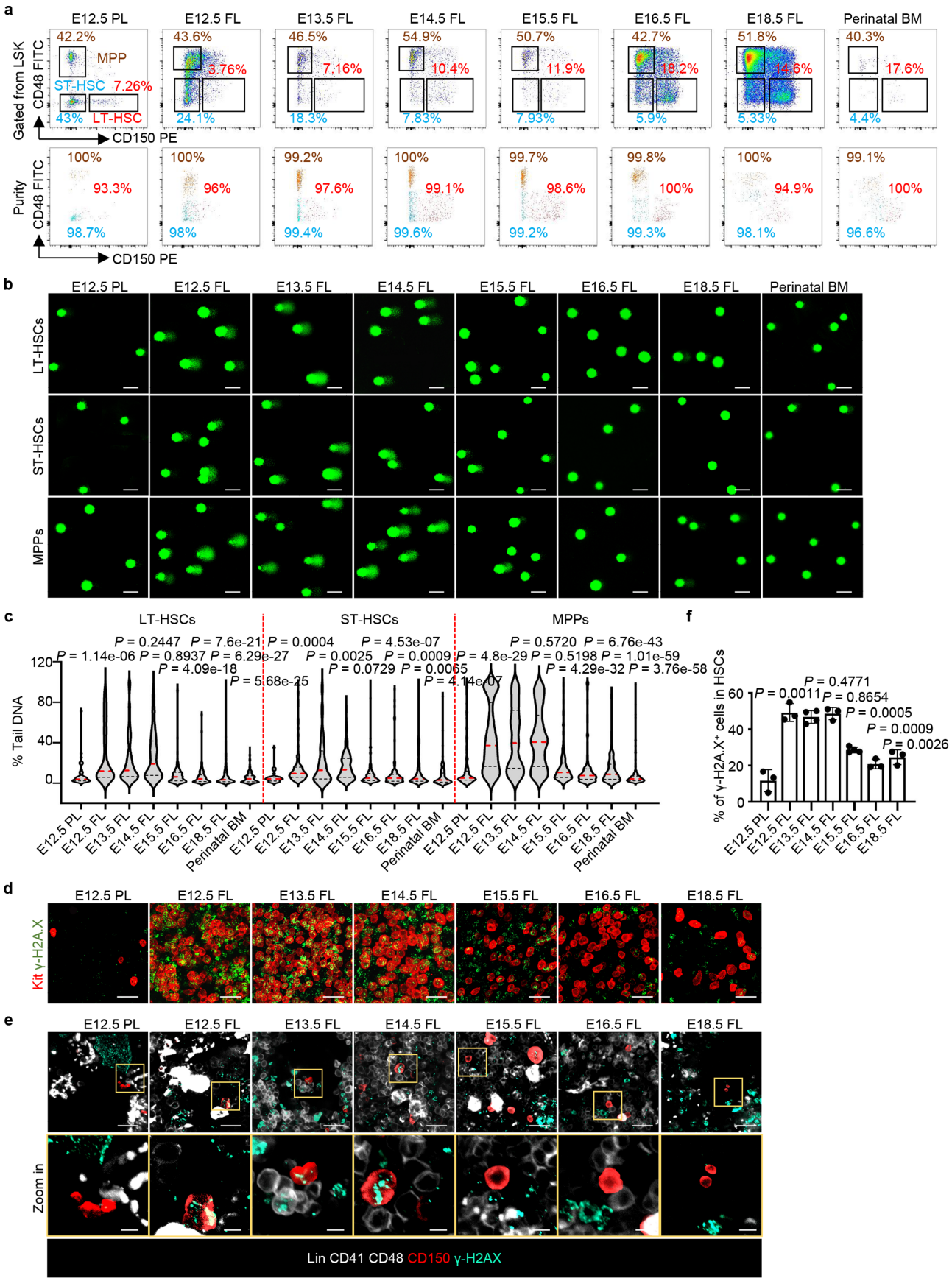

Extended Data Fig. 2 | See next page for caption.

Extended Data Fig. 2 | Flow-sorting of HSCs and MPPs and DNA damage detection after Eto-treatment ex vivo or in vivo. a, LT-HSCs ($LSKCD150^{+}CD48^{-}$), ST-HSCs ($LSKCD150^{-}CD48^{-}$), and MPPs ($LSKCD150^{-}CD48^{+}$) were sorted by flow cytometry with high purities from the haematopoietic tissues labelled to assay their sensitivity to genotoxic agents ($n = 3$ per group). **b, c**, Representative comet-tail DNA images and proportions induced by Eto-treatment ex vivo in LT-HSCs, ST-HSCs and MPPs isolated from the labelled tissues ($n = 3$ per group). The medians (red dashed lines) and quartiles (black dashed lines) of each group are shown. Scale bar, 50 µm. **d**, Representative in situ fluorescence images of Kit and γ-H2AX after Eto-treatment in vivo (E12.5 PL, E12.5 FL, $n = 5$; E13.5 FL, E16.5 FL, $n = 4$; E14.5 FL, E15.5 FL, E18.5 FL, $n = 3$). Scale bar, 30 µm. **e, f**, Representative in situ fluorescence images and the positive cell proportion of γ-H2AX in HSCs ($Lin^{-}CD41^{-}CD48^{-}CD150^{+}$) after Eto-treatment in vivo (E13.5 FL, E15.5 FL, $n = 4$, other groups, $n = 3$; mean ± s.d.). Scale bars, 20 and 5 µm. The *n* represents individual samples (**a**-**c**) and fetuses (**d**-**f**) from 3 independent experiments. Statistical tests: unpaired two-sided Student's t-test (**c, f**).

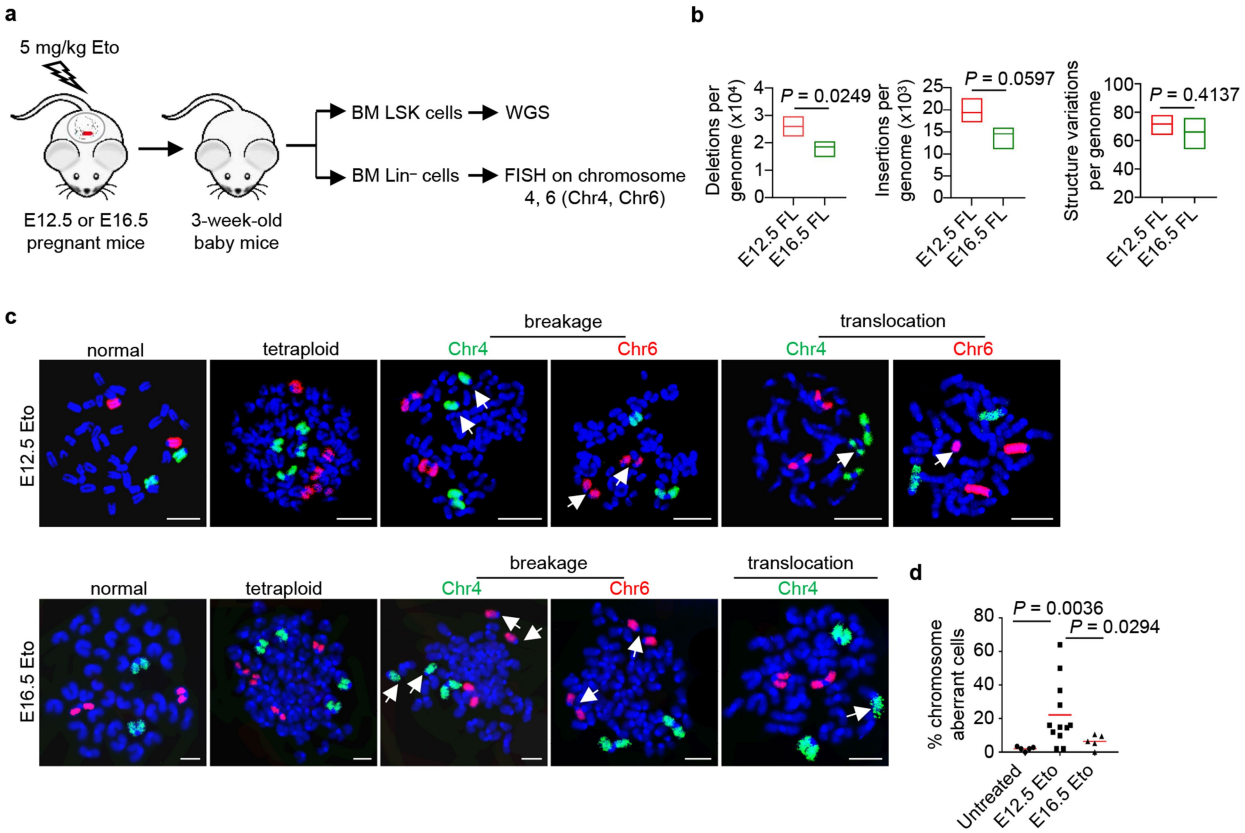

Extended Data Fig. 3 | Chromosomal alterations in BM HSPCs from Eto-treated mice at the embryonic stage. a, Experimental design for whole-genome sequencing (WGS) and chromosome fluorescence in situ hybridization (FISH). **b**, The genome mutation numbers in 3-week-old BM-LSK cells (E12.5 FL, $n = 3$; E16.5 FL, $n = 4$). The boxes delimit the minima and maxima, and the horizontal line represents the mean. **c, d**, Representative fluorescence images and proportions of normal and aberrant chromosomes in cells from mice treated with Eto at E12.5 or E16.5, chromosome 4 (FITC) and chromosome 6 (Texas red); arrows indicate aberrant chromosomes (Untreated, $n = 6$, E12.5 Eto, $n = 15$; E16.5 Eto, $n = 5$; mean ± s.d.). Scale bar, 10 μm. The n represents individual samples (**b**) and mice (**c, d**) from 3 independent experiments. Statistical tests: unpaired two-sided Student's t-test (**b**), unpaired one-sided Student's t-test with Welsh's correction (**d**).

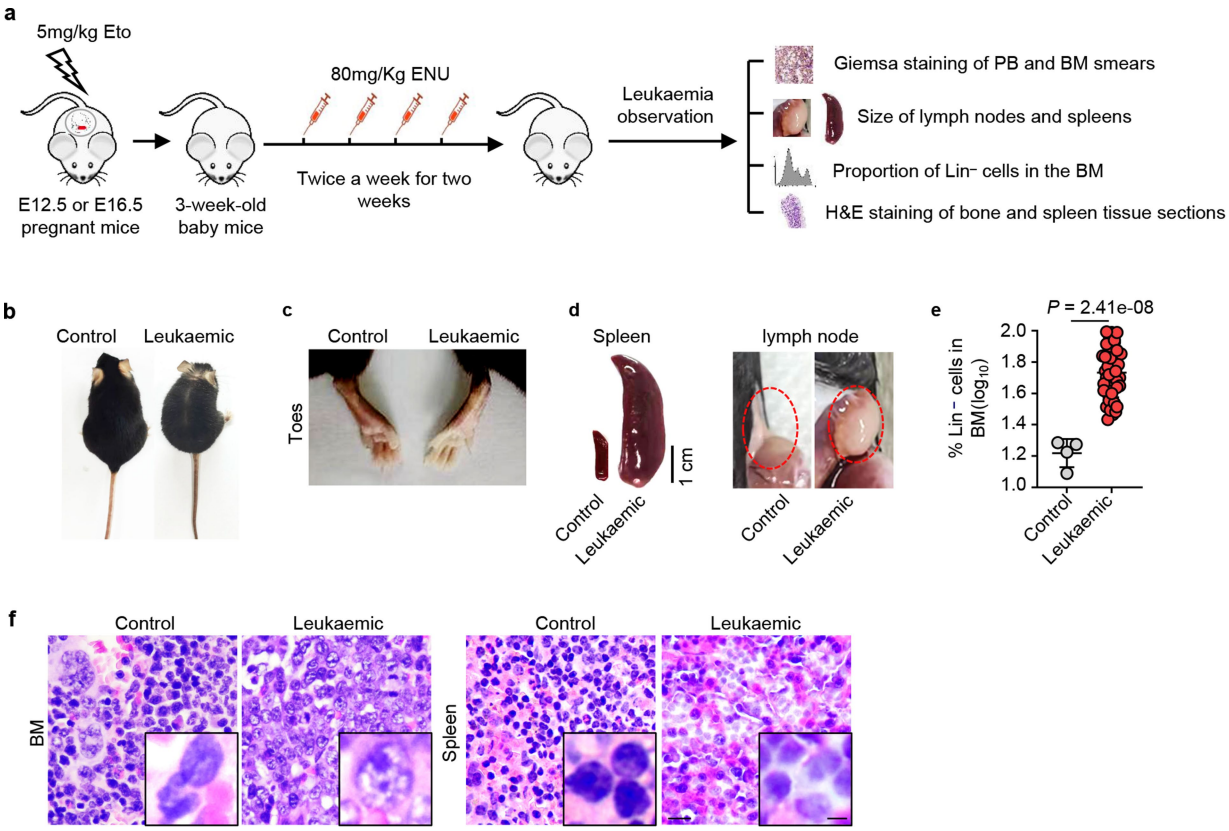

Extended Data Fig. 4 | Leukaemia induction and observation in mice. **a**, Experimental design for leukaemia induction and monitoring in mice. ENU, N-ethyl-N-nitrosourea; PB, peripheral blood; BM, bone marrow. **b, c**, The physical symptoms of leukaemic and normal control mice. **d**, Spleens and lymph nodes from leukaemic and control mice. **b**-**d**, Control, $n = 5$, Leukaemic, $n = 51$. **e**, The proportion of lineage-negative cells in the BM of leukaemic and control mice (Control, $n = 5$, Leukaemic, $n = 51$; mean ± s.d.). **f**, Representative H&E images of tissue sections (Control, $n = 4$; Leukaemic, $n = 10$). Scale bars, 100 and 25 μm. The n represents individual mice. Statistical tests: unpaired two-sided Student's t-test (**e**).

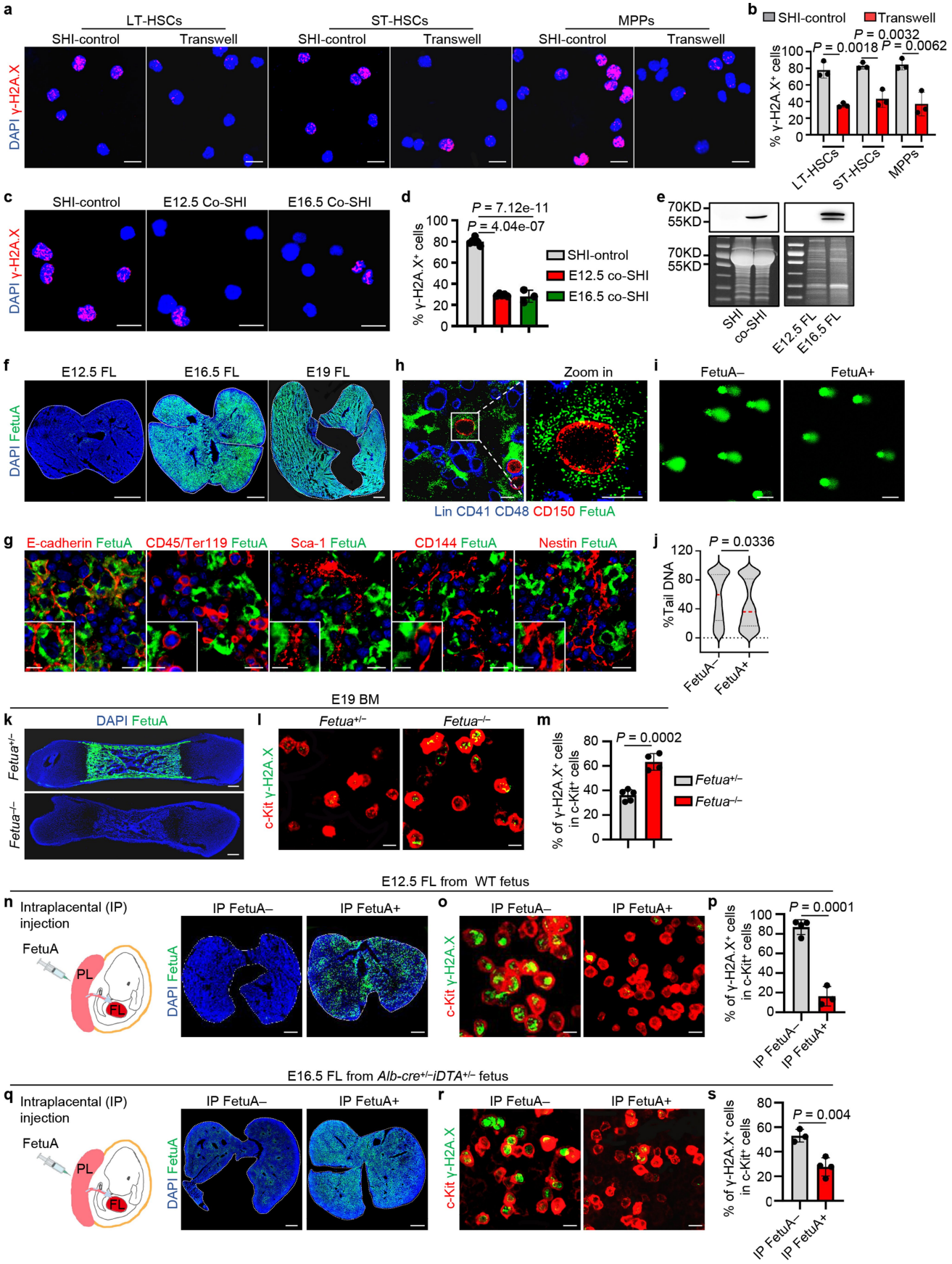

Extended Data Fig. 5 | See next page for caption.

Extended Data Fig. 5 | The hepatocyte-secreted factor FetuA provides genome protection for HSPCs. a, b, Representative fluorescence images and positive proportions of γ-H2AX induced by Eto in E12.5 FL LT-HSCs, ST-HSCs and MPPs cultured with or without hepatocytes (refer to Fig. 3a) ($n = 3$). Scale bar, 20 μm. **c, d**, Representative fluorescence images and positive proportions of γ-H2AX Eto-induced in E12.5 FL-HSPCs in cultures of E16.5 or E12.5 hepatocyte-conditioned medium (co-SHI) or basic medium (SHI) (SHI-control, $n = 6$, E12.5 Co-SHI, $n = 3$; E16.5 Co-SHI, $n = 5$). Scale bar, 20 μm. **e**, Western-blots analysis of FetuA in SHI and co-SHI media and in E12.5 and E16.5 FL tissues; Coomassie blue was used as a loading control ($n = 3$). **f**, Representative fluorescence images of FetuA in E12.5 FL, E16.5 FL and E19 FL ($n = 3$). Scale bar, 500 μm. **g**, Representative fluorescence images of FetuA and hepatocytes (E-cadherin$^+$), haematopoietic (CD45/Ter119$^+$), endothelial (Scal-1 or CD144$^+$), mesenchymal (Nestin$^+$) cells in E16.5 FL ($n = 3$). Scale bars, 10 and 5 μm. **h**, Representative fluorescence images of FetuA (green) and HSPCs (Lin$^-$CD41$^-$CD48$^-$CD150$^+$) in E16.5 FL ($n = 3$). Scale bars, 10 and 5 μm. **i, j**, Representative comet-tail DNA images and the proportions of Eto-induced tail DNA in HSPCs cultured with or without FetuA ($n = 3$). The medians (red dashed lines) and quartiles (black dashed lines) of each group are shown. Scale bar, 100 μm. **k**, Representative fluorescence images of FetuA in the E19 bone marrow (BM) of *Fetua*$^{+/-}$ and *Fetua*$^{-/-}$ mice. Scale bar, 500 μm. **l, m**, Representative fluorescence images and positive cell proportions of γ-H2AX (green) in Kit$^+$ cells (red) in the E19 BM of *Fetua*$^{+/-}$ or *Fetua*$^{-/-}$ mice ($n = 3$). Scale bar, 10 μm. **n**, Representative fluorescence images of FetuA in the E12.5 FL of mice with or without intraplacental (IP) injection of FetuA. Scale bar, 300 μm. **o, p**, Representative fluorescence images and positive cell proportions of γ-H2AX (green) in Kit$^+$ cells (red) in the E12.5 FL of mice with or without IP injection of FetuA followed by Eto-treatment in vivo (IP FetuA−, $n = 4$; IP FetuA+, $n = 3$). Scale bar, 10 μm. **q**, Representative fluorescence images of FetuA in the E16.5 FL of Alb-cre; ROSA26-LSL-DTA mice with or without IP injection of FetuA. Scale bar, 500 μm. **r, s**, Representative fluorescence images and positive cell proportions of γ-H2AX (green) in Kit$^+$ cells (red) in the E16.5 FL of Alb-cre; ROSA26-LSL-DTA mice with or without IP injection of FetuA followed by Eto-treatment in vivo (IP FetuA−, $n = 3$; IP FetuA+, $n = 4$). Scale bar, 10 μm. The n represents independent experiments (**a**-**j**) and fetuses (**k**-**s**) from 3 independent experiments. The mean ± s.d. is shown (**b, d, m, p, s**). Statistical tests: unpaired two-sided Student's t-test (**b, d, j, m, p, s**).

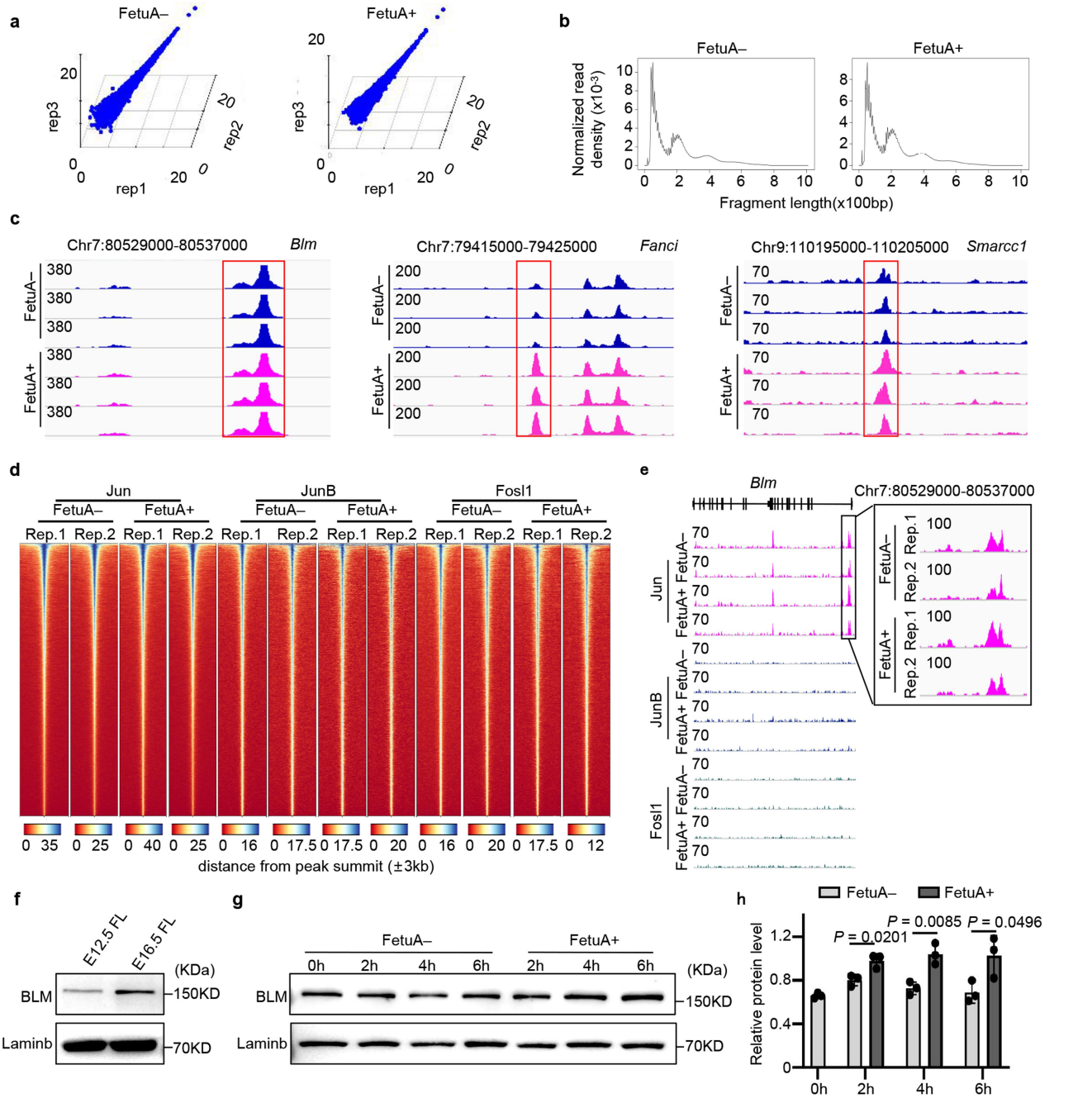

Extended Data Fig. 6 | Effects of FetuA on HSPCs. a, Scatter-plots showing the consistency of ATAC-seq replicates for each group ($n = 3$). **b**, Fragment size distribution of ATAC-seq data ($n = 3$). **c**, ATAC-seq signals of *Blm*, *Fanci* and *Smarcc1* in Integrative Genomics Viewer are shown; the red boxes indicate the peaks where the bZIP motifs are located ($n = 3$). **d**, Heatmaps showing the Cut & Tag peak signal intensities ($n = 2$). **e**, Cut & Tag sequencing signals of Jun, JunB and Fosl1 on the *Blm* gene from the Integrative Genomics Viewer are shown ($n = 2$). Cut & Tag for Jun binding to the *Blm* promoter. **f**, Western-blots analysis of the BLM protein in LSK cells from E12.5 FL and E16.5 FL ($n = 2$). **g, h**, Western-blots and relative signal intensity of the BLM protein in Lin$^-$ cells cultured with or without FetuA at different time points ($n = 3$; mean ± s.d.). The *n* represents independent experiments. Statistical tests: unpaired two-sided Student's t-test (**h**).

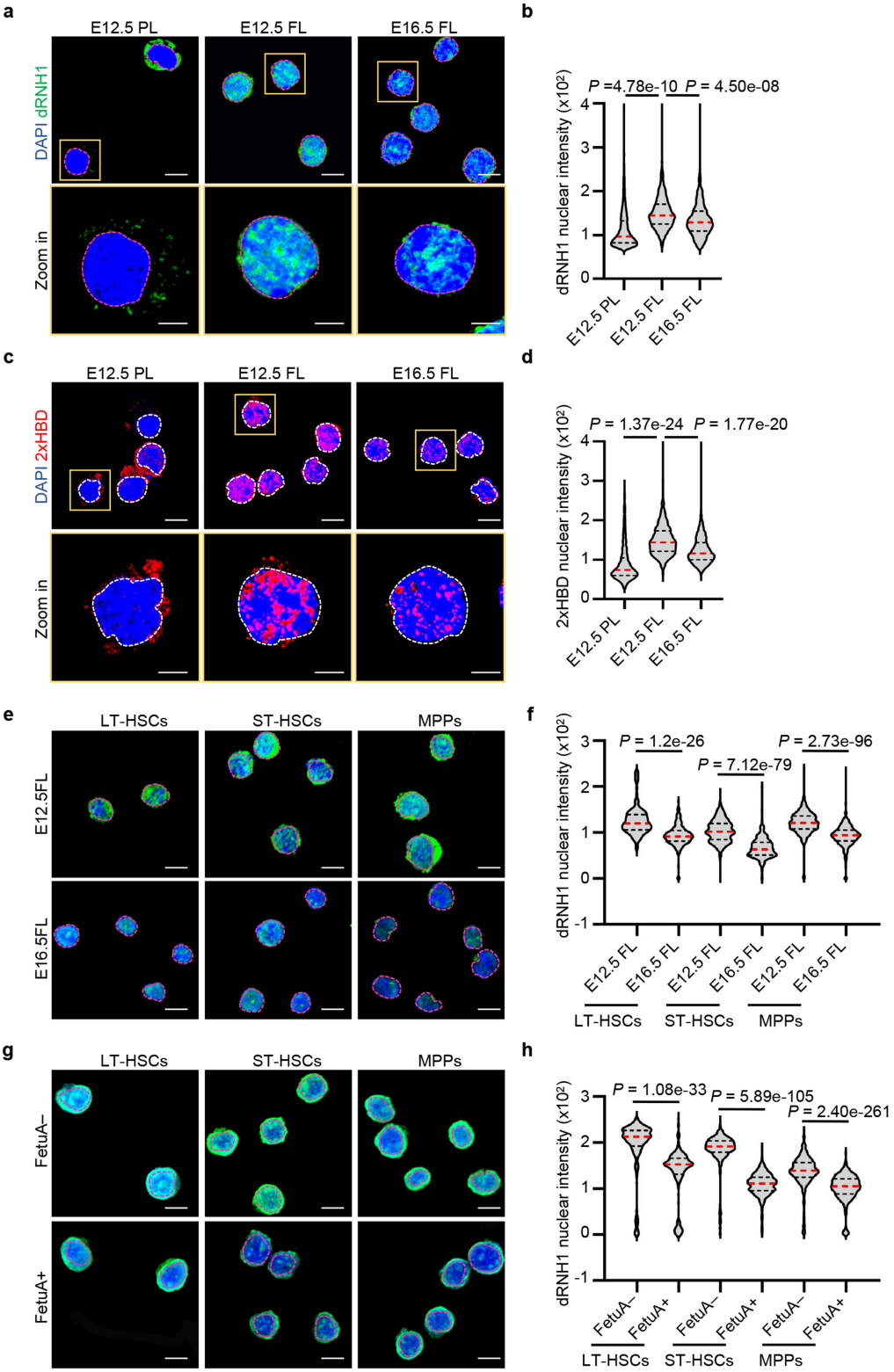

Extended Data Fig. 7 | Immunofluorescence assay of dRNH1 and 2xHBD in HSPCs. a, b, Representative fluorescence images and nuclear intensity of dRNH1 in HSPCs from E12.5 PL, E12.5 FL and E16.5 FL ($n = 3$). Scale bars, 10 and 5 μm. **c, d**, Representative fluorescence images and nuclear intensity of 2xHBD in HSPCs from E12.5 PL, E12.5 FL and E16.5 FL ($n = 3$). Scale bars, 10 and 5 μm. **e, f**, Representative fluorescence images and nuclear intensity of dRNH1 in HSCs and MPPs from E12.5 FL and E16.5 FL ($n = 3$). Scale bar, 10 μm. **g, h**, Representative fluorescence images and nuclear signal intensity of dRNH1 in E12.5 FL HSCs and MPPs cultured with or without FetuA ($n = 3$). Scale bar, 10 μm. The nuclear regions are circled by dotted lines (**a, c, e, g**). The medians (red dashed lines) and quartiles (black dashed lines) are shown (**b, d, f, h**). The *n* represents independent experiments. Statistical tests: unpaired two-sided Student's t-test (**b, d, f, h**).

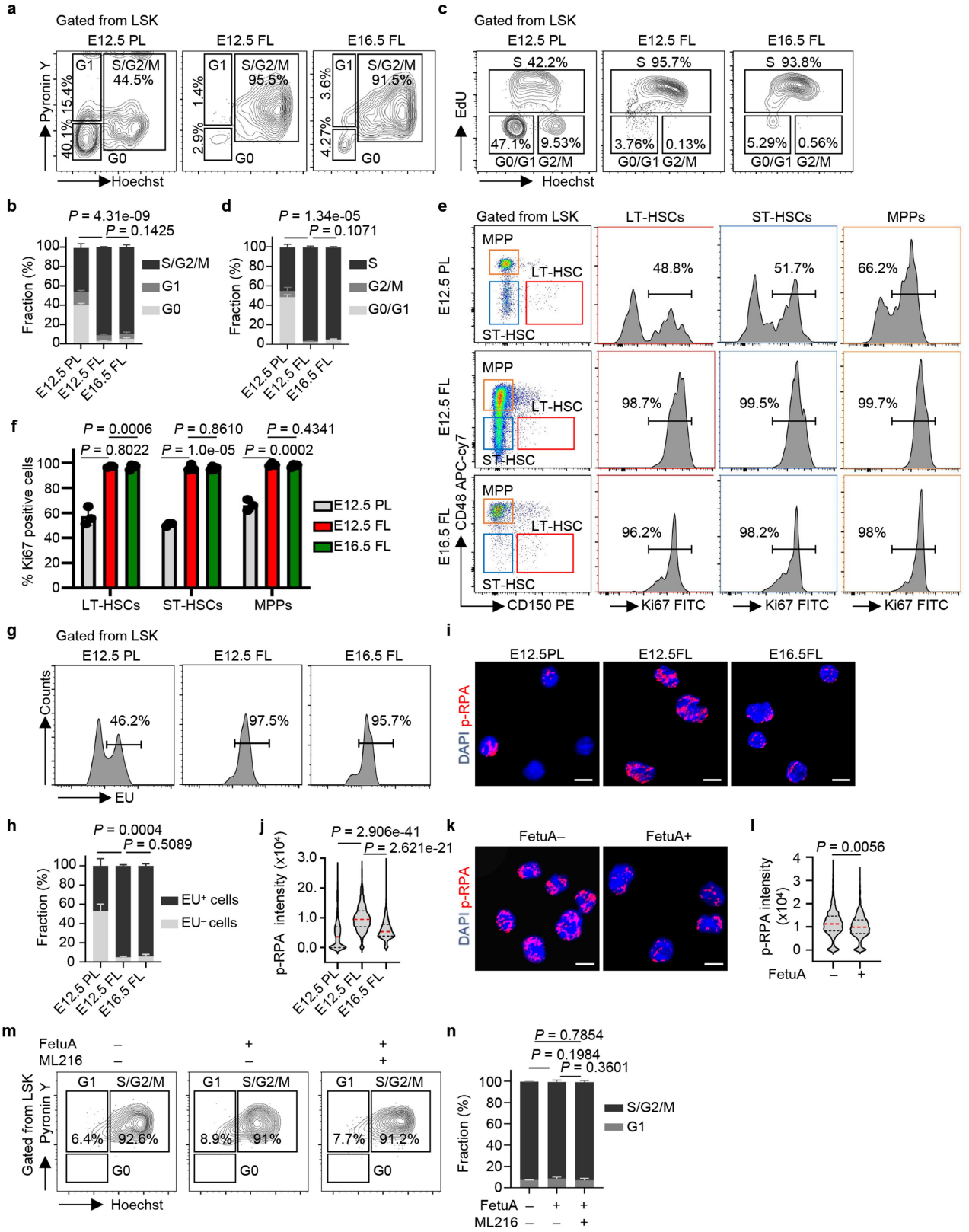

Extended Data Fig. 8 | See next page for caption.

Extended Data Fig. 8 | Fetal liver HSPCs undergo DNA-replication and transcription simultaneously. a, b, Representative flow cytometry images and the proportions of each cell cycle stage in HSPCs from E12.5 PL, E12.5 FL and E16.5 FL cells stained with Hoechst 33342 and PyroninY (E12.5 PL, E16.5 FL, $n = 3$; E12.5 FL, $n = 6$; S/G2/M phase was compared). **c, d**, Representative flow cytometry images and the proportions of HSPCs in each cell cycle stage at E12.5 PL, E12.5 FL and E16.5 FL after 5-ethynyl-2′-deoxyuridine (EdU) treatment ($n = 3$ per group; S phase was compared). **e, f**, Representative flow cytometry images and Ki67-positive cell proportions in HSCs and MPPs from E12.5PL, E12.5FL and E16.5FL ($n = 3$ per group). **g, h**, Representative flow cytometry images and the ethyluridine (EU)-positive fraction of HSPCs from E12.5 PL, E12.5 FL and E16.5 FL after EU-treatment (E12.5 PL, E12.5 FL, $n = 3$; E16.5 FL, $n = 6$; EU^+ population was compared). **i, j**, Representative fluorescence images and nuclear signal intensity of p-RPA in HSPCs from E12.5 PL, E12.5 FL and E16.5 FL ($n = 3$). The medians (red dashed lines) and quartiles (black dashed lines) are shown. Scale bar, 10 μm. **k, l**, Representative fluorescence images and nuclear signal intensity of p-RPA in E12.5 FL-HSPCs treated with or without FetuA ($n = 3$). The medians (red dashed lines) and quartiles (black dashed lines) are shown. Scale bar, 10 μm. **m, n**, Representative flow cytometry images and the proportion of each cell cycle stage in HSPCs cultured with or without FetuA and the BLM inhibitor ML216 ($n = 3$). The mean ± s.d. is shown (**b, d, f, h, n**). The *n* represents individual samples from 3 independent experiments (**a**-**h**) and independent experiments (**i**-**n**). Statistical tests: unpaired two-sided Student's t-test (**b, d, f, h, j, l, n**).

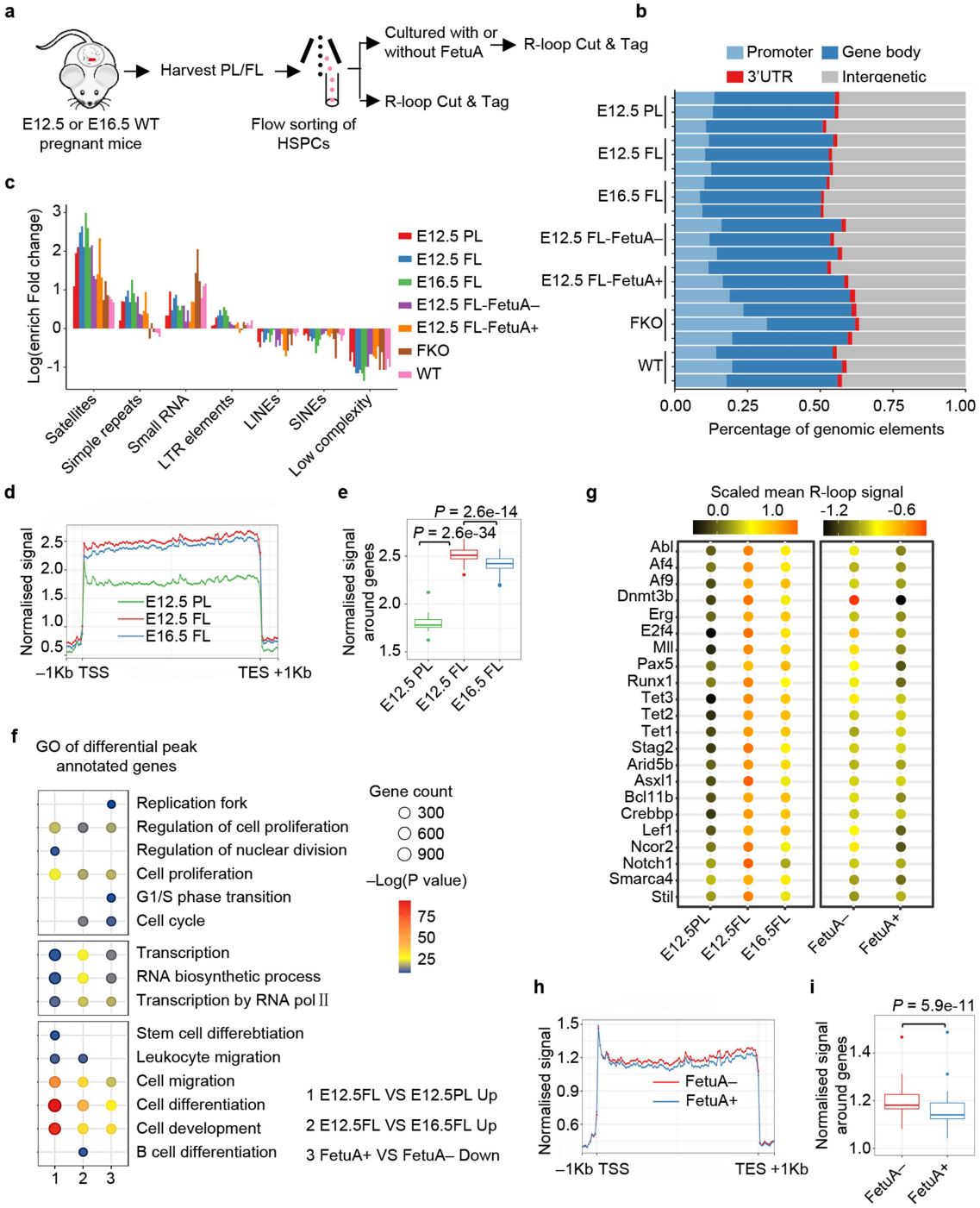

Extended Data Fig. 9 | Genome-wide R-loop and DNA sequencing assays of fetal HSPCs. a, Experimental design for genome-wide R-loop sequencing (R-loop Cut & Tag). **b**, Genomic distribution of R-loop peaks in each sample. **c**, Enrichment of R-loops in various types of repetitive elements in each sample. **d**, Gene-metaplots analysis of R-loop Cut & Tag; mean coverages of R-loop signals over gene bodies (±1 kb) in the HSPCs from E12.5 PL, E12.5 FL and E16.5 FL are shown. **e**, Box-plots showing the R-loop signal over gene bodies (±1 kb) in HSPCs from E12.5PL, E12.5 FL and E16.5 FL. The boxes delimit the lower (25th) and upper (75th) interquartile, and the horizontal line represents the median. **f**. GO analysis of differentially expressed peak-annotated genes; the circle size shows the number of genes associated with each GO term, and the circle colour denotes the −Log (*P* value). **g**, Mean R-loop signal of the genes that are frequently involved in leukemogenesis in HSPCs from E12.5 PL, E12.5 FL, and E16.5 FL and in E12.5 FL HSPCs cultured with or without FetuA. **h**, Gene-metaplots analysis of R-loop Cut & Tag; mean coverages of R-loop signals over gene bodies (±1 kb) in E12.5 FL HSPCs cultured with or without FetuA are shown. **i**, Box-plots showing the R-loop signal over gene bodies (± 1 kb) in E12.5 FL HSPCs cultured with or without FetuA. The boxes delimit the lower (25th) and upper (75th) interquartile, and the horizontal line represents the median. $n = 3$ independent experiments (**b**-**i**). Statistical tests: two-sided Wilcoxon test (**e**, **i**).

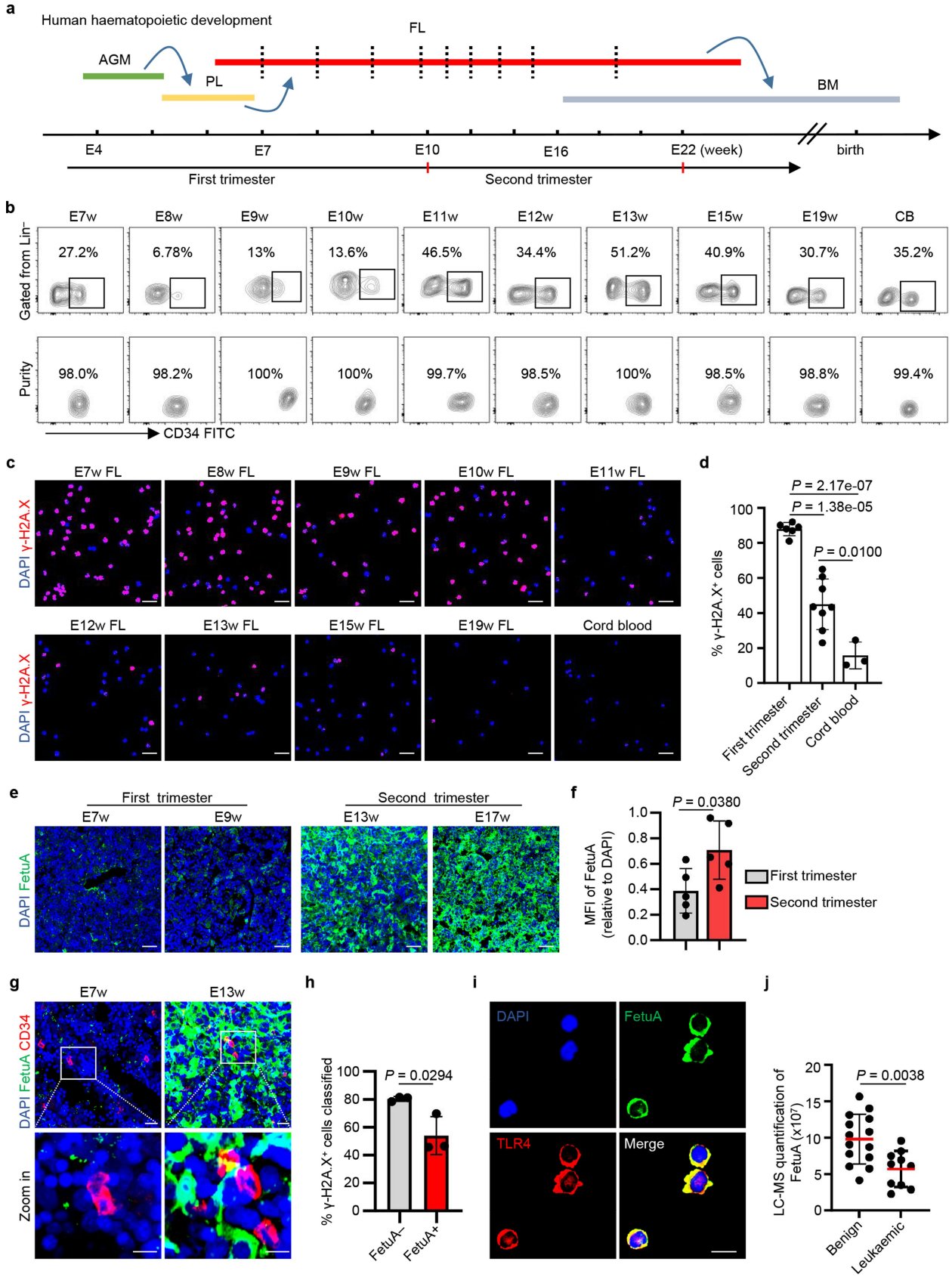

Extended Data Fig. 10 | See next page for caption.

Extended Data Fig. 10 | Similar genome-protective mechanism in humans. **a**, Schematic of haematopoietic development and the tissues used for HSPC harvest (red dashed lines) for the assessment of genome stability. **b**, Immunophenotypically lineage-negative (Lin^-) and CD34-positive ($CD34^+$) cells were flow-sorted with high purities from the haematopoietic tissue of E7w fetal liver (FL), E8w FL, E9w FL, E10w FL, E11w FL, E12w FL, E13w FL, E15w FL, E16w FL and neonatal cord blood (CB) to determine the sensitivity of HSPCs to genotoxic agents. **c, d**, Representative fluorescence images and positive proportions of γ-H2AX induced by Eto in human HSPCs isolated from FL and CB (first trimester, $n = 6$; second trimester, $n = 8$; cord blood, $n = 3$). Scale bar, 50 μm. **e, f**, Representative fluorescence images and mean fluorescence intensity (MFI) of FetuA (green) in human FL at the indicated developmental stages ($n = 5$ per group). Scale bar, 50 μm. **g**, Representative fluorescence images of FetuA and CD34 (red) in FL ($n = 3$). Upper scale bar, 20 μm; lower scale bar, 10 μm. **h**, Proportions of γ-H2AX-positive FL-HSPCs cultured with or without FetuA induced by Eto in the first trimester ($n = 3$). **i**, Representative fluorescence images of FetuA and TLR4 on HSPCs after FetuA-treatment ($n = 3$). Scale bar, 20 μm. **j**, Liquid chromatography-mass spectrometry quantification of FetuA in the bone marrow blood sera of benign and leukaemic infants (Benign, $n = 14$; Leukaemic, $n = 10$). The n represents individual samples (**c-f, j**) and independent experiments (**g-i**). The mean ± s.d. is shown (**d, f, h, j**). Statistical tests: unpaired two-sided Student's t-test (**d, f, h, j**).

nature portfolio

Corresponding author(s): Dengli Hong

Last updated by author(s): Sep 12, 2024

Reporting Summary

Nature Portfolio wishes to improve the reproducibility of the work that we publish. This form provides structure for consistency and transparency in reporting. For further information on Nature Portfolio policies, see our Editorial Policies and the Editorial Policy Checklist.

Statistics

For all statistical analyses, confirm that the following items are present in the figure legend, table legend, main text, or Methods section.

n/a	Confirmed	
☐	☒	The exact sample size (*n*) for each experimental group/condition, given as a discrete number and unit of measurement
☐	☒	A statement on whether measurements were taken from distinct samples or whether the same sample was measured repeatedly
☐	☒	The statistical test(s) used AND whether they are one- or two-sided *Only common tests should be described solely by name; describe more complex techniques in the Methods section.*
☐	☒	A description of all covariates tested
☐	☒	A description of any assumptions or corrections, such as tests of normality and adjustment for multiple comparisons
☐	☒	A full description of the statistical parameters including central tendency (e.g. means) or other basic estimates (e.g. regression coefficient) AND variation (e.g. standard deviation) or associated estimates of uncertainty (e.g. confidence intervals)
☐	☒	For null hypothesis testing, the test statistic (e.g. *F*, *t*, *r*) with confidence intervals, effect sizes, degrees of freedom and *P* value noted *Give P values as exact values whenever suitable.*
☒	☐	For Bayesian analysis, information on the choice of priors and Markov chain Monte Carlo settings
☒	☐	For hierarchical and complex designs, identification of the appropriate level for tests and full reporting of outcomes
☒	☐	Estimates of effect sizes (e.g. Cohen's *d*, Pearson's *r*), indicating how they were calculated

Our web collection on statistics for biologists contains articles on many of the points above.

Software and code

Policy information about availability of computer code

Data collection	BD FACSDiva(V8.0.3), Summit (V6.3.1.16945), Las X (V4.7), ZEN (V2.3)
Data analysis	ImageJ(V1.52p), OpenComet(V1.3.1), Imaris (V9.0.1), FlowJo(V10), Graphpad Pism (V9.5.0), Trim_Galore(V0.6.7), IGV(V2.7.0), Bowtie2(V2.3.5.1), Burrow-Wheeler Aligner(V0.7.17), ATAC-seq QC (V1.14.4), DESeq2 (V1.26.0), HOMER(V4.11), hisat2 (V2.2.1), Picard(V2.25.5), deepTools(V3.5.1), MACS2(V2.2.6), R package ChIPseeker(V1.22.1), clusterProfiler(V3.14.3), circlise(V0.4.8), complex Heatmap package(V2.2.0), STAR(V2.7), HTSeq-count (V0.13.5), R (V3.6.3), HALO(V3.6.4134).

For manuscripts utilizing custom algorithms or software that are central to the research but not yet described in published literature, software must be made available to editors and reviewers. We strongly encourage code deposition in a community repository (e.g. GitHub). See the Nature Portfolio guidelines for submitting code & software for further information.

Data

Policy information about availability of data

All manuscripts must include a data availability statement. This statement should provide the following information, where applicable:

- Accession codes, unique identifiers, or web links for publicly available datasets
- A description of any restrictions on data availability
- For clinical datasets or third party data, please ensure that the statement adheres to our policy

The ATAC sequencing, RNA sequencing, R-loop Cut & Tag sequencing, b-ZIPs Cut & Tag sequencing and whole genome sequencing data reported in this paper have

been deposited at the Genome Sequence Archive in BIG Data Center, Beijing Institute of Genomics (BIG), Chinese Academy of Sciences, under the study accession number PRJCA026810, accessible link: http://ngdc.cncb.ac.cn/bioproject/browse/ PRJCA026810. The reference genome used is mm10, accessible link: https://hgdownload.soe.ucsc.edu/goldenPath/mm10/bigZips/mm10.fa.gz. The annotation dataset used in RNA sequencing analysis is gencode.vM25.annotation.gtf, accessible link: http://ftp.ebi.ac.uk/pub/databases/gencode/Gencode_mouse/release_M25/gencode.vM25.annotation.gtf.gz.

Research involving human participants, their data, or biological material

Policy information about studies with human participants or human data. See also policy information about sex, gender (identity/presentation), and sexual orientation and race, ethnicity and racism.

Reporting on sex and gender	Our study was not related to sex and gender, so the sex and gender were not considered. Eleven foetal liver samples , 3 cord blood samples, 14 bone marrow plasma samples from begnin infants, 10 bone marrow plasma samples from leukaemic infants were used in this study.
Reporting on race, ethnicity, or other socially relevant groupings	Socailly relevant categorization variables were not used in my manuscript.
Population characteristics	The foetal liver samples were collected from foetus (7-week-old, n=1; 8-week-old, n=3; 9-week-old, n=1; 10-week-old, n=1; 11-week-old, n=1; 13-week-old, n=1; 15-week-old, n=1; 16-week-old, n=1; 19-week-old, n=1). Cord blood samples were collected from placenta of new born babies. The bone marrow plasma samples were collected from 0-12-month-old patients (benign group: 2-month-old, n=1; 3-month-old, n=2; 4-month-old, n=2; 5-month-old, n=3; 6-month-old, n=3; 8-month-old, n=1; 9-month-old, n=1, 12-mpmth-old, n=1; leukaemic group: 2-month-old, n=2; 3-month-old, n=1; 4-month-old, n=2; 6-month-old, n=1; 8-month-old, n=1; 9-month-old, n=2; 11-month-old, n=1). Available samples were used without any selection.
Recruitment	The foetal liver samples were collected randomly from fetus by induced abortion at different gastational age. The cord blood samples were collected randomly from the plancenta of new born babies. The bone marrow plasma samples were collected from 0-12 month old infants and then seperated into begnin and leukaemia group accroding to their diagnostic reports.
Ethics oversight	Medical Ethics Committee of Tongji Hospital, Tongji University School of Medicine, Shanghai, China (k-w-2010-010). Medical Ethics Committee of Shanghai Children's Medical Center, Shanghai Jiao Tong University School of Medicine, Shanghai, China (SCMCIRB-K2024163-1).

Note that full information on the approval of the study protocol must also be provided in the manuscript.

Field-specific reporting

Please select the one below that is the best fit for your research. If you are not sure, read the appropriate sections before making your selection.

☒ Life sciences ☐ Behavioural & social sciences ☐ Ecological, evolutionary & environmental sciences

For a reference copy of the document with all sections, see nature.com/documents/nr-reporting-summary-flat.pdf

Life sciences study design

All studies must disclose on these points even when the disclosure is negative.

Sample size	No sample size calculation was performed. Sample size was chosen based on the statistical requirements. The exact sample sizes are included in the figure legends.
Data exclusions	No data were excluded.
Replication	A detailed experimental protocol is provided for replcation by others.The comet assay, rh2a.x staining, flow-sorting, tissue immunofluorescence, hepatocytes culture, cell cycle analysis were replicated at least 2 experimenters with reproducible results. All the experiments were independently repeated at least three times with reproducible results.
Randomization	All the samples were allocated into experimental groups randomly.
Blinding	In our study, most experimental findings were related to comparative analysis. For comparative experiments, the groups were treated at different conditions, the investigators can not be blinded to the group allocation. However, most data collection and analysis were automatically completed by the software, there is low likelihood of investigator's bias in the final readout. For the experiment of leukaemic model, the investigators were blinded to the group allocation of FetuA ko and wild type control mice, but the data analysis were not blinded because we needed the genotype to identify different group.

Behavioural & social sciences study design

All studies must disclose on these points even when the disclosure is negative.

Study description	*Briefly describe the study type including whether data are quantitative, qualitative, or mixed-methods (e.g. qualitative cross-sectional, quantitative experimental, mixed-methods case study).*
Research sample	*State the research sample (e.g. Harvard university undergraduates, villagers in rural India) and provide relevant demographic information (e.g. age, sex) and indicate whether the sample is representative. Provide a rationale for the study sample chosen. For studies involving existing datasets, please describe the dataset and source.*
Sampling strategy	*Describe the sampling procedure (e.g. random, snowball, stratified, convenience). Describe the statistical methods that were used to predetermine sample size OR if no sample-size calculation was performed, describe how sample sizes were chosen and provide a rationale for why these sample sizes are sufficient. For qualitative data, please indicate whether data saturation was considered, and what criteria were used to decide that no further sampling was needed.*
Data collection	*Provide details about the data collection procedure, including the instruments or devices used to record the data (e.g. pen and paper, computer, eye tracker, video or audio equipment) whether anyone was present besides the participant(s) and the researcher, and whether the researcher was blind to experimental condition and/or the study hypothesis during data collection.*
Timing	*Indicate the start and stop dates of data collection. If there is a gap between collection periods, state the dates for each sample cohort.*
Data exclusions	*If no data were excluded from the analyses, state so OR if data were excluded, provide the exact number of exclusions and the rationale behind them, indicating whether exclusion criteria were pre-established.*
Non-participation	*State how many participants dropped out/declined participation and the reason(s) given OR provide response rate OR state that no participants dropped out/declined participation.*
Randomization	*If participants were not allocated into experimental groups, state so OR describe how participants were allocated to groups, and if allocation was not random, describe how covariates were controlled.*

Ecological, evolutionary & environmental sciences study design

All studies must disclose on these points even when the disclosure is negative.

Study description	*Briefly describe the study. For quantitative data include treatment factors and interactions, design structure (e.g. factorial, nested, hierarchical), nature and number of experimental units and replicates.*
Research sample	*Describe the research sample (e.g. a group of tagged Passer domesticus, all Stenocereus thurberi within Organ Pipe Cactus National Monument), and provide a rationale for the sample choice. When relevant, describe the organism taxa, source, sex, age range and any manipulations. State what population the sample is meant to represent when applicable. For studies involving existing datasets, describe the data and its source.*
Sampling strategy	*Note the sampling procedure. Describe the statistical methods that were used to predetermine sample size OR if no sample-size calculation was performed, describe how sample sizes were chosen and provide a rationale for why these sample sizes are sufficient.*
Data collection	*Describe the data collection procedure, including who recorded the data and how.*
Timing and spatial scale	*Indicate the start and stop dates of data collection, noting the frequency and periodicity of sampling and providing a rationale for these choices. If there is a gap between collection periods, state the dates for each sample cohort. Specify the spatial scale from which the data are taken*
Data exclusions	*If no data were excluded from the analyses, state so OR if data were excluded, describe the exclusions and the rationale behind them, indicating whether exclusion criteria were pre-established.*
Reproducibility	*Describe the measures taken to verify the reproducibility of experimental findings. For each experiment, note whether any attempts to repeat the experiment failed OR state that all attempts to repeat the experiment were successful.*
Randomization	*Describe how samples/organisms/participants were allocated into groups. If allocation was not random, describe how covariates were controlled. If this is not relevant to your study, explain why.*
Blinding	*Describe the extent of blinding used during data acquisition and analysis. If blinding was not possible, describe why OR explain why blinding was not relevant to your study.*

Did the study involve field work? ☐ Yes ☐ No

Field work, collection and transport

Field conditions	*Describe the study conditions for field work, providing relevant parameters (e.g. temperature, rainfall).*
Location	*State the location of the sampling or experiment, providing relevant parameters (e.g. latitude and longitude, elevation, water depth).*
Access & import/export	*Describe the efforts you have made to access habitats and to collect and import/export your samples in a responsible manner and in compliance with local, national and international laws, noting any permits that were obtained (give the name of the issuing authority, the date of issue, and any identifying information).*
Disturbance	*Describe any disturbance caused by the study and how it was minimized.*

Reporting for specific materials, systems and methods

We require information from authors about some types of materials, experimental systems and methods used in many studies. Here, indicate whether each material, system or method listed is relevant to your study. If you are not sure if a list item applies to your research, read the appropriate section before selecting a response.

Materials & experimental systems

n/a	Involved in the study
☐	☒ Antibodies
☒	☐ Eukaryotic cell lines
☒	☐ Palaeontology and archaeology
☐	☒ Animals and other organisms
☒	☐ Clinical data
☒	☐ Dual use research of concern
☒	☐ Plants

Methods

n/a	Involved in the study
☒	☐ ChIP-seq
☐	☒ Flow cytometry
☒	☐ MRI-based neuroimaging

Antibodies

Antibodies used	CD34 FITC(581) BD 555821, Biotin-labled lineage markers ThermoFisher 88-7774-75, Sca-1 PE-cy7(D7) ThermoFisher 25-5981-82, c-Kit APC (2B8) ThermoFisher 17-1171-82, CD150 PE(mShad150) ThermoFisher 12-1502-82, CD48 FITC(HM48-1) ThermoFisher 11-0481-82, Phosphor-histone H2A.X(ser139)(20E3) rabbit mAb cell signaling technology(CST) 9718s, Tlr4 antibody abcam ab13556, FetuinA antibody(EPR17839-163) abcam ab187051, p-RPA(phopho s33) abccam ab211877, Tlr4 antibody(UT41) ThermoFisher 53-9041-80, huamn FetuinA antibody(1F6B9) Proteintech 66094-1-Ig, Myd88(E11) Santa Cruz sc-74532, anti-mouse CD117(ACK2) ThermoFisher 14-1172-85, Ter119 APC Biolegend 116212, Gr-1 APC Biolegend 108412, Mac-1 APC Biolegend 101212, B220 APC Biolegend 103212, CD3 APC Biolegend 100236, CD150 BV421(SLAM) Biolegend 115925, CD41 APC(MWRag30) Biolegend 133913, c-Kit goat mAb R&D AF1356, E-cadherin rabbit monoclonal antibdoy(24E10) CST 3195T, anti-huamn albumin antibody(MAB1455) R&D 188835, laminin monoclonal antibody Abcam ab11575, Ki67-FITC(SolA15) ThermoFisher 11-5698-80, CD34 antibody(EP373Y) Abcam ab81289, anti-p-junb(Thr102/Thr104) CST 8053S, anti-p-fosl1(s265) CST 3880S, anti-p-cjun(phopho s63), Abcam ab32385, anti-junb (EPR6518) Abcam ab128878, anti-fosl1 Abcam ab232745, anti-c-jun(EP693Y) Abcam ab40766, anti-laminB1(EPR8985) Abcam ab133741, anti-FetuinA(EPR17839-163) Abcam ab187051, anti-Blm(B-4) santa cruz sc-365753, c-Jun rabbit mAb (60A8) CST 9165T, Junb rabbit mAb(C37F9) CST 3753S, Fosl1 mouse mAb(c-12) santa cruz sc-28310, dRNH1 antibody, 2xHBD antibody, CD45 FITC(104) Invitrogen MCD45201, Nestin antibody Beyotime AN205-1, E-cadherin antibody(DECAM-1) Santa Cruz sc-59778, CD144 antibody BD 550548, Sca-1 antibody (D7) BD 557403, FITC-labelled Sca-1(E13-161.7) biolegend 122506, APC-cy7-labelled CD48 (HM48-1) BioLegend, 103431, FITC-labelled Ki-67(SolA15) ThermoFisher, 11-5698-80.
Validation	The dRNH1 antbody and 2xHBD antibody were validated by previous articles with the following links: dRNH1 antibody:https://doi.org/10.1083/jcb.202101092 2xHBD antibody:https://www.science.org/doi/10.1126/sciadv.abe3516 Antibody validation information can be found at the manufacturer's website with the following links: CD34 FITC(581) BD 555821:https://www.bdbiosciences.com/zh-cn/products/reagents/flow-cytometry-reagents/research-reagents/single-color-antibodies-ruo/fitc-mouse-anti-human-cd34.555821 Biotin-labled lineage markers ThermoFisher Sca-1 PE-cy7(D7) ThermoFisher 25-5981-82: https://www.thermofisher.cn/cn/zh/antibody/product/Ly-6A-E-Sca-1-Antibody-clone-D7-Monoclonal/25-5981-82 c-Kit APC (2B8) ThermoFisher 17-1171-82:https://www.thermofisher.cn/cn/zh/antibody/product/CD117-c-Kit-Antibody-clone-2B8-Monoclonal/17-1171-82 CD150 PE(mShad150) ThermoFisher 12-1502-82:https://www.thermofisher.cn/cn/zh/antibody/product/CD150-Antibody-clone-mShad150-Monoclonal/12-1502-82 CD48 FITC(HM48-1) ThermoFisher 11-0481-82:https://www.thermofisher.cn/cn/zh/antibody/product/CD48-Antibody-clone-HM48-1-Monoclonal/11-0481-82 Phosphor-histone H2A.X(ser139)(20E3) rabbit mAb cell signaling technology(CST) 9718s:https://www.cellsignal.cn/products/primary-antibodies/phospho-histone-h2a-x-ser139-20e3-rabbit-mab/9718 Tlr4 antibody abcam ab13556:https://www.abcam.cn/products/primary-antibodies/tlr4-antibody-ab13556.html

FetuinA antibody(EPR17839-163) abcam ab187051:https://www.abcam.cn/products/primary-antibodies/ahsg-antibody-epr17839-163-ab187051.html
p-RPA(phopho s33) abccam ab211877:https://www.abcam.cn/products/primary-antibodies/rpa32rpa2-phospho-s33-antibody-ab211877.html
Tlr4 antibody(UT41) ThermoFisher 53-9041-80:https://www.thermofisher.cn/antibody/product/53-9041-80.html?CID=AFLLS-53-9041-80
huamn FetuinA antibody(1F6B9) Proteintech 66094-1-Ig:https://www.ptglab.com/Products/AHSG-Antibody-66094-1-Ig.htm
Myd88(E11) Santa Cruz sc-74532:https://www.scbt.com/zh/p/myd88-antibody-e-11
anti-mouse CD117(ACK2) ThermoFisher 14-1172-85:https://www.thermofisher.cn/cn/zh/antibody/product/CD117-c-Kit-Antibody-clone-ACK2-Monoclonal/14-1172-85
Ter119 APC Biolegend 116212:https://www.biolegend.com/en-us/products/apc-anti-mouse-ter-119-erythroid-cells-antibody-1863
Gr-1 APC Biolegend 108412:https://www.biolegend.com/en-us/products/apc-anti-mouse-ly-6g-ly-6c-gr-1-antibody-456
Mac-1 APC Biolegend 101212:https://www.biolegend.com/en-us/products/apc-anti-mouse-human-cd11b-antibody-345
B220 APC Biolegend 103212:https://www.biolegend.com/en-us/products/apc-anti-mouse-human-cd45r-b220-antibody-442
CD3 APC Biolegend 100236:https://www.biolegend.com/en-us/products/apc-anti-mouse-cd3-antibody-8055
CD150 BV421(SLAM) Biolegend 115925:https://www.biolegend.com/en-us/products/brilliant-violet-421-anti-mouse-cd150-slam-antibody-7162
CD41 APC(MWRag30) Biolegend 133913:https://www.biolegend.com/en-us/products/apc-anti-mouse-cd41-antibody-7592
c-Kit goat mAb R&D AF1356:https://www.rndsystems.com/cn/products/human-mouse-cd117-c-kit-antibody_af1356
E-cadherin rabbit monoclonal antibdoy(24E10) CST 3195T:https://www.cellsignal.cn/products/primary-antibodies/e-cadherin-24e10-rabbit-mab/3195
anti-huamn albumin antibody(MAB1455) R&D 188835:https://www.rndsystems.com/cn/products/human-serum-albumin-antibody-188835_mab1455
laminin monoclonal antibody Abcam ab11575:https://www.abcam.cn/products/primary-antibodies/laminin-antibody-ab11575.html
Ki67-FITC(SolA15) ThermoFisher 11-5698-80:https://www.thermofisher.cn/cn/zh/antibody/product/Ki-67-Antibody-clone-SolA15-Monoclonal/11-5698-80
CD34 antibody(EP373Y) Abcam ab81289:https://www.abcam.cn/products/primary-antibodies/cd34-antibody-ep373y-ab81289.html
anti-p-junb(Thr102/Thr104) CST 8053S:https://www.cellsignal.cn/products/primary-antibodies/phospho-junb-thr102-thr104-d3c6-rabbit-mab/8053
anti-p-fosl1(s265) CST 3880S:https://www.cellsignal.cn/products/primary-antibodies/phospho-fra1-ser265-antibody/3880
anti-p-cjun(phopho s63) Abcam ab32385:https://www.abcam.cn/products/primary-antibodies/c-jun-phospho-s63-antibody-y172-ab32385.html
anti-junb (EPR6518) Abcam ab128878:https://www.abcam.cn/products/primary-antibodies/junb-antibody-epr6518-ab128878.html
anti-fosl1 Abcam ab232745:https://www.abcam.cn/products/primary-antibodies/fra1-antibody-ab232745.html
anti-c-jun(EP693Y) Abcam ab40766:https://www.abcam.cn/products/primary-antibodies/c-jun-antibody-ep693y-ab40766.html
anti-laminB1(EPR8985) Abcam ab133741:https://www.abcam.cn/products/primary-antibodies/lamin-b1-antibody-epr8985b-nuclear-envelope-marker-ab133741.html
anti-FetuinA(EPR17839-163) Abcam ab187051:https://www.abcam.cn/products/primary-antibodies/ahsg-antibody-epr17839-163-ab187051.html
anti-Blm(B-4) santa cruz sc-365753:https://www.scbt.com/zh/p/blm-antibody-b-4
c-Jun rabbit mAb (60A8) CST 9165T:https://www.cellsignal.cn/products/primary-antibodies/c-jun-60a8-rabbit-mab/9165
Junb rabbit mAb(C37F9) CST 3753S:https://www.cellsignal.cn/products/primary-antibodies/junb-c37f9-rabbit-mab/3753
Fosl1 mouse mAb(c-12) santa cruz sc-28310:https://www.scbt.com/zh/p/fra-1-antibody-c-12
CD45 FITC(104) Invitrogen MCD45201:https://www.thermofisher.cn/cn/zh/antibody/product/CD45-2-Antibody-Monoclonal/MCD45201?imageId=2517
Nestin antibody Beyotime AN205-1:https://www.beyotime.com/product/AN205.htm
E-cadherin antibody(DECAM-1) Santa Cruz sc-59778:https://www.scbt.com/zh/p/e-cadherin-antibody-decma-1
CD144 antibody BD 550548:https://www.bdbiosciences.com/zh-cn/products/reagents/flow-cytometry-reagents/research-reagents/single-color-antibodies-ruo/purified-rat-anti-mouse-cd144.550548
Sca-1 antibody (D7) BD 557403:https://www.bdbiosciences.com/zh-cn/products/reagents/flow-cytometry-reagents/research-reagents/single-color-antibodies-ruo/purified-rat-anti-mouse-ly-6a-e.557403
FITC-labelled Sca-1(E13-161.7) biolegend 122506: https://www.biolegend.com/ja-jp/products/fitc-anti-mouse-ly-6a-e-sca-1-antibody-3894?GroupID=BLG5162
APC-cy7-labelled CD48 (HM48-1) BioLegend, 103431:https://www.biolegend.com/ja-jp/products/apc-cyanine7-anti-mouse-cd48-antibody-8054
FITC-labelled Ki-67(SolA15) ThermoFisher, 11-5698-80: https://www.thermofisher.cn/cn/zh/antibody/product/Ki-67-Antibody-clone-SolA15-Monoclonal/11-5698-80

Eukaryotic cell lines

Policy information about cell lines and Sex and Gender in Research

Cell line source(s)	*State the source of each cell line used and the sex of all primary cell lines and cells derived from human participants or vertebrate models.*
Authentication	*Describe the authentication procedures for each cell line used OR declare that none of the cell lines used were authenticated.*
Mycoplasma contamination	*Confirm that all cell lines tested negative for mycoplasma contamination OR describe the results of the testing for mycoplasma contamination OR declare that the cell lines were not tested for mycoplasma contamination.*
Commonly misidentified lines (See ICLAC register)	*Name any commonly misidentified cell lines used in the study and provide a rationale for their use.*

Palaeontology and Archaeology

Specimen provenance	*Provide provenance information for specimens and describe permits that were obtained for the work (including the name of the issuing authority, the date of issue, and any identifying information). Permits should encompass collection and, where applicable, export.*
Specimen deposition	*Indicate where the specimens have been deposited to permit free access by other researchers.*
Dating methods	*If new dates are provided, describe how they were obtained (e.g. collection, storage, sample pretreatment and measurement), where they were obtained (i.e. lab name), the calibration program and the protocol for quality assurance OR state that no new dates are provided.*

☐ Tick this box to confirm that the raw and calibrated dates are available in the paper or in Supplementary Information.

Ethics oversight	*Identify the organization(s) that approved or provided guidance on the study protocol, OR state that no ethical approval or guidance was required and explain why not.*

Note that full information on the approval of the study protocol must also be provided in the manuscript.

Animals and other research organisms

Policy information about studies involving animals; ARRIVE guidelines recommended for reporting animal research, and Sex and Gender in Research

Laboratory animals	C57BL/6J, Cg-Tg(Alb-cre)21Mgn/J, B6.Cg-Gt(ROSA)26Sortm14(CAG-tdTomato)Hze/J, B6.129P2-Gt(ROSA)26Sortm1(DTA)Ly/J, C57BL/6JGpt-FetuinA ko(cas9). Mice were maintained and bred in a specific pathogen-free facility in ventilated cages, a maximum of 5 mice per cage, on a 12-hour day-night cycle, at 20-26 °C and 30-70% humidity. For embryo collection, 8–10-week-old male and female were used. For the proportion analysis of LSK, CFC, whole genome sequencing, chromosome FISH and leukaemic model, 3-week-old mice were used.
Wild animals	No wild animals were used in this study.
Reporting on sex	The sex was not considered in our study design. About 500 mice were used in the study.
Field-collected samples	No field-collected samples were used in this study.
Ethics oversight	Animal procedures for mice were approved by the Scientific Investigation Board of Shanghai Jiao Tong University School of Medicine, Shanghai, china.

Note that full information on the approval of the study protocol must also be provided in the manuscript.

Clinical data

Policy information about clinical studies

All manuscripts should comply with the ICMJE guidelines for publication of clinical research and a completed CONSORT checklist must be included with all submissions.

Clinical trial registration	*Provide the trial registration number from ClinicalTrials.gov or an equivalent agency.*
Study protocol	*Note where the full trial protocol can be accessed OR if not available, explain why.*
Data collection	*Describe the settings and locales of data collection, noting the time periods of recruitment and data collection.*
Outcomes	*Describe how you pre-defined primary and secondary outcome measures and how you assessed these measures.*

Dual use research of concern

Policy information about dual use research of concern

Hazards

Could the accidental, deliberate or reckless misuse of agents or technologies generated in the work, or the application of information presented in the manuscript, pose a threat to:

No	Yes	
☐	☐	Public health
☐	☐	National security
☐	☐	Crops and/or livestock
☐	☐	Ecosystems
☐	☐	Any other significant area

Experiments of concern

Does the work involve any of these experiments of concern:

No	Yes	
☐	☐	Demonstrate how to render a vaccine ineffective
☐	☐	Confer resistance to therapeutically useful antibiotics or antiviral agents
☐	☐	Enhance the virulence of a pathogen or render a nonpathogen virulent
☐	☐	Increase transmissibility of a pathogen
☐	☐	Alter the host range of a pathogen
☐	☐	Enable evasion of diagnostic/detection modalities
☐	☐	Enable the weaponization of a biological agent or toxin
☐	☐	Any other potentially harmful combination of experiments and agents

Plants

Seed stocks	*Report on the source of all seed stocks or other plant material used. If applicable, state the seed stock centre and catalogue number. If plant specimens were collected from the field, describe the collection location, date and sampling procedures.*
Novel plant genotypes	*Describe the methods by which all novel plant genotypes were produced. This includes those generated by transgenic approaches, gene editing, chemical/radiation-based mutagenesis and hybridization. For transgenic lines, describe the transformation method, the number of independent lines analyzed and the generation upon which experiments were performed. For gene-edited lines, describe the editor used, the endogenous sequence targeted for editing, the targeting guide RNA sequence (if applicable) and how the editor was applied.*
Authentication	*Describe any authentication procedures for each seed stock used or novel genotype generated. Describe any experiments used to assess the effect of a mutation and, where applicable, how potential secondary effects (e.g. second site T-DNA insertions, mosiacism, off-target gene editing) were examined.*

ChIP-seq

Data deposition

☐ Confirm that both raw and final processed data have been deposited in a public database such as GEO.

☐ Confirm that you have deposited or provided access to graph files (e.g. BED files) for the called peaks.

Data access links *May remain private before publication.*	*For "Initial submission" or "Revised version" documents, provide reviewer access links. For your "Final submission" document, provide a link to the deposited data.*
Files in database submission	*Provide a list of all files available in the database submission.*
Genome browser session (e.g. UCSC)	*Provide a link to an anonymized genome browser session for "Initial submission" and "Revised version" documents only, to enable peer review. Write "no longer applicable" for "Final submission" documents.*

Methodology

Replicates	*Describe the experimental replicates, specifying number, type and replicate agreement.*
Sequencing depth	*Describe the sequencing depth for each experiment, providing the total number of reads, uniquely mapped reads, length of reads and whether they were paired- or single-end.*
Antibodies	*Describe the antibodies used for the ChIP-seq experiments; as applicable, provide supplier name, catalog number, clone name, and lot number.*
Peak calling parameters	*Specify the command line program and parameters used for read mapping and peak calling, including the ChIP, control and index files used.*

Data quality	*Describe the methods used to ensure data quality in full detail, including how many peaks are at FDR 5% and above 5-fold enrichment.*
Software	*Describe the software used to collect and analyze the ChIP-seq data. For custom code that has been deposited into a community repository, provide accession details.*

Flow Cytometry

Plots

Confirm that:

☒ The axis labels state the marker and fluorochrome used (e.g. CD4-FITC).

☒ The axis scales are clearly visible. Include numbers along axes only for bottom left plot of group (a 'group' is an analysis of identical markers).

☒ All plots are contour plots with outliers or pseudocolor plots.

☒ A numerical value for number of cells or percentage (with statistics) is provided.

Methodology

Sample preparation	The murine mononuclear cells used for sorting or cell cycle analysis were isolated from placenta, foetal liver or bone marrow at different developmental stages. The tissues were dissected into single-cell suspensions, then incubated with antibodies. After staining, the cells were washed and resuspended in ice cold MACS for sorting or analysis. The human mononuclear cells used for sorting were isolated from foetal liver or cord blood. The foetal livers were dissected into single cell suspensions, then the mononuclear cells from foetal liver or cord blood were separated using Ficoll density gradient centrifugation. Lineage-positive cells were depleted using the MagniSort Human haematopoietic lineage depletion kit. Lineage-negative cells were then incubated with antibodies. After staining, the cells were washed and resuspended in ice cold MACS for sorting.
Instrument	BD FACSAria3, MoFlo Astrios, cytoFLEX LX.
Software	FlowJo_v10
Cell population abundance	Purity of sorted populations was assessed by post-sort analysis. Purity of over 95% was routinel achieved.
Gating strategy	For murine HSPCs: The first gate excluded any cellular debris based on FSC-A vs SSC-A. These cells were then sub-gated to identify only single cells, based on removal of outliers from the SSC-W vs SSC-H plot. lineage-negative cells were isolated by gating for cells with the lowest expression of lineage panel of antibodies (B220, CD3, Gr-1, Ter119, lineage-PE, or lineage Percp-cy5.5 or Lineage-APC-cy7). Sca-1+c-Kit+ cells were gated based on a high expression of Sca-1 and c-Kit (Sca-1-PE-cy7 vs c-Kit-APC). Within the Sca-1+c-Kit+ population, the gates for LT-HSCs (CD150+CD48-), ST-HSCs (CD150-CD48-), MPPs (CD150-CD48+) (CD150-PE vs CD48-FITC) were defined. For cell cycle analysis: the HSPCs used for the cell cycle analysis were gated as above. Then the final gate was defined based on the Hochest vs Pyronin Y, Hochest vs EdU-FITC, Ki67-PE vs SSA. For human HSPCs: The first gate excluded any cellular debris based on FSC-A vs SSC-A. These cells were then sub-gated to identify only single cells, based on removal of outliers from the SSC-W vs SSC-H plot. Lineage-negative cells were isolated by gating for cells with lowest expression of lineage panel antibodies(CD2, CD3, CD10, CD11b, CD14, CD16, CD19, CD56, CD123, CD235a, lineage-PE), within lineage-negative population, the CD34+ cells were gated based on a high expression of CD34(CD34-FITC vs SSC-A).

☒ Tick this box to confirm that a figure exemplifying the gating strategy is provided in the Supplementary Information.

Magnetic resonance imaging

Experimental design

Design type	*Indicate task or resting state; event-related or block design.*
Design specifications	*Specify the number of blocks, trials or experimental units per session and/or subject, and specify the length of each trial or block (if trials are blocked) and interval between trials.*
Behavioral performance measures	*State number and/or type of variables recorded (e.g. correct button press, response time) and what statistics were used to establish that the subjects were performing the task as expected (e.g. mean, range, and/or standard deviation across subjects).*

Acquisition

Imaging type(s) *Specify: functional, structural, diffusion, perfusion.*

Field strength *Specify in Tesla*

Sequence & imaging parameters *Specify the pulse sequence type (gradient echo, spin echo, etc.), imaging type (EPI, spiral, etc.), field of view, matrix size, slice thickness, orientation and TE/TR/flip angle.*

Area of acquisition *State whether a whole brain scan was used OR define the area of acquisition, describing how the region was determined.*

Diffusion MRI ☐ Used ☐ Not used

Preprocessing

Preprocessing software *Provide detail on software version and revision number and on specific parameters (model/functions, brain extraction, segmentation, smoothing kernel size, etc.).*

Normalization *If data were normalized/standardized, describe the approach(es): specify linear or non-linear and define image types used for transformation OR indicate that data were not normalized and explain rationale for lack of normalization.*

Normalization template *Describe the template used for normalization/transformation, specifying subject space or group standardized space (e.g. original Talairach, MNI305, ICBM152) OR indicate that the data were not normalized.*

Noise and artifact removal *Describe your procedure(s) for artifact and structured noise removal, specifying motion parameters, tissue signals and physiological signals (heart rate, respiration).*

Volume censoring *Define your software and/or method and criteria for volume censoring, and state the extent of such censoring.*

Statistical modeling & inference

Model type and settings *Specify type (mass univariate, multivariate, RSA, predictive, etc.) and describe essential details of the model at the first and second levels (e.g. fixed, random or mixed effects; drift or auto-correlation).*

Effect(s) tested *Define precise effect in terms of the task or stimulus conditions instead of psychological concepts and indicate whether ANOVA or factorial designs were used.*

Specify type of analysis: ☐ Whole brain ☐ ROI-based ☐ Both

Statistic type for inference *Specify voxel-wise or cluster-wise and report all relevant parameters for cluster-wise methods.*

(See Eklund et al. 2016)

Correction *Describe the type of correction and how it is obtained for multiple comparisons (e.g. FWE, FDR, permutation or Monte Carlo).*

Models & analysis

n/a	Involved in the study
☐	☐ Functional and/or effective connectivity
☐	☐ Graph analysis
☐	☐ Multivariate modeling or predictive analysis

Functional and/or effective connectivity *Report the measures of dependence used and the model details (e.g. Pearson correlation, partial correlation, mutual information).*

Graph analysis *Report the dependent variable and connectivity measure, specifying weighted graph or binarized graph, subject- or group-level, and the global and/or node summaries used (e.g. clustering coefficient, efficiency, etc.).*

Multivariate modeling and predictive analysis *Specify independent variables, features extraction and dimension reduction, model, training and evaluation metrics.*